View Article Online
View Journal

Green Chemistry

Cutting-edge research for a greener sustainable future

Accepted Manuscript

This article can be cited before page numbers have been issued, to do this please use: W. Lang, J. Deng, X. Liu, Z. Yang, R. Zhang, H. Liu, K. Sun and S. Yuan, *Green Chem.*, 2025, DOI: 10.1039/D5GC02932E.

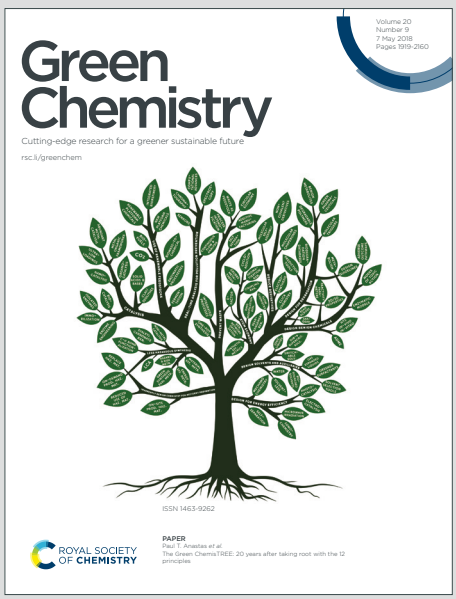

ROYAL SOCIETY OF CHEMISTRY

rsc.li/greenchem

View Article Online
DOI: 10.1039/D5GC02932E

Green Foundation

1. This study elucidates the molecular structure of coke deposits during biomass pyrolysis, their formation mechanism, and their impact on catalytic reactions, providing a theoretical foundation for mitigating catalyst deactivation, reducing regeneration frequency, and lowering CO_2 emissions. These insights advance sustainable H_2 production from biomass, aligning with green chemistry principles of waste minimization and energy efficiency.
2. We identify the five-membered ring structure in "soft" coke deposits, extending beyond traditional physical morphology analyses to clarify how molecular configurations influence catalyst deactivation and tar conversion. A comprehensive coke formation mechanism at the molecular level is proposed.
3. Future work should focus on optimizing catalyst supports and minimizing metal usage to design coke-resistant catalysts that controllably modulate deposit structures.

View Article Online
DOI: 10.1039/D5GC02932E

Unveiling the Five-Membered Ring Structures in "Soft" Coke Deposits on Fe-Ni Catalysts: Formation Mechanisms and Implications for Biomass Catalytic Reforming

*Wenkai Lang[a, #], Jin Deng[a, #], Xin Liu[b], Zaiyu Yang[a], Ruxia Zhang[a], Honghong Liu[a], Keyuan Sun[a, *], Shenfu Yuan[a, *]*

[a] School of Chemical Science and Engineering, Institute of International Rivers and Eco-security, Key Laboratory of Medicinal Chemistry for Natural Resource, Ministry of Education, National Center for Experimental Chemistry and Chemical Engineering Education Demonstration, Yunnan Provincial Key Laboratory of Carbon Neutral and Green Low-Carbon Technology, Yunnan University, Kunming, China.

[b] Dawei Hengyuan Chemical Co., Ltd., Qujing, China.

Abstract: Coke deposits on catalysts during the reforming of biomass pyrolysis volatiles are usually the primary cause of catalyst deactivation and a major challenge for catalyst design. Unlike simple graphite carbon layers, coke deposits consist of complex macromolecular compounds, making it difficult to elucidate their structural features and formation mechanisms at the molecular level. In this work, based on the pyrolysis of wheat straw in a fixed-bed reactor followed by catalytic reforming of volatiles over Fe-Ni catalysts to produce H_2-rich syngas, the pyrolysis-gas

* Corresponding author.

E-mail address: yuanshenfu@ynu.edu.cn, sunkeyuan@stu.ynu.edu.cn

#These authors contribute equally to this work.

View Article Online
DOI: 10.1039/D5GC02932E

chromatography/mass spectrometry (Py-GC/MS) was employed to analyze fragmented molecules derived from the pyrolysis of coke deposits. The chemical structure of coke deposits containing five-membered rings was demonstrated for the first time by backward induction. Fast pyrolysis experiments demonstrated the interactions between primary volatiles and the catalyst, while fixed-bed scaled-up experiments combined with multiphase product analysis demonstrated the role of the catalyst in the formation of the coke deposits. The results showed that the catalyst support guided the adsorption of volatiles and the deposition of carbonaceous species, while metal sites promoted cyclization and polymerization reactions. Coke deposits with different chemical structures contribute differently to catalyst deactivation. Compared to "hard" coke deposits dominated by graphitic carbon, "soft" coke deposits characterized by five-membered ring structures were not the main cause of catalyst deactivation and could continue to convert tar. Model compound studies pinpointed cyclopentenone, a cellulose/hemicellulose pyrolysis derivative, as a key intermediate for the assembly of five-membered ring structures in coke deposits. The reaction pathways and mechanisms of coke formation were further elucidated by combining experimental and theoretical calculations. This study provides some insights for the structural analysis and formation mechanisms of coke deposits on catalysts.

1. Introduction

Humanity is facing the dual challenges of energy crisis and environmental pollution. The excessive consumption of fossil fuels not only leads to resource depletion

View Article Online
DOI: 10.1039/D5GC02932E

but also causes severe environmental problems, such as greenhouse gas emissions and air pollution.[1] In this context, there is an urgent need to explore alternative energy sources to replace traditional fossil fuels. Biomass, the only renewable resource containing carbon, possesses vast reserves but remains underutilized. Much biomass originates from agricultural waste, and its indiscriminate accumulation or direct combustion poses safety hazards and causes environmental pollution. Pyrolysis offers a promising approach to convert biomass into clean hydrogen energy, reducing reliance on fossil fuels and addressing energy and environmental challenges.[2] To enhance H_2 yield and minimize harmful byproducts such as tar, catalytic reforming of biomass pyrolysis volatiles using catalysts is essential.[3] Fe-Ni bimetallic catalysts have been widely used due to their affordability and excellent catalytic activity.[4] However, compared to sintering and sulfur poisoning, catalyst deactivation caused by coke deposits remains the most significant challenge in catalytic reforming.[5] Deactivated catalysts lead to low reaction efficiency, poor biomass utilization, and increased harmful byproducts. Frequent catalyst replacement raises operational costs and reduces process economics. Moreover, the regeneration of used catalysts requires heating in an oxygen-containing atmosphere, resulting in additional CO_2 emissions and energy consumption.[6] Therefore, the development of coke-resistant catalysts to improve stability and longevity while reducing the frequency of replacement and regeneration is essential for the clean utilization of biomass, environmental mitigation, and energy sustainability. Investigating the structure and formation mechanisms of coke deposits on catalysts, as well as understanding the influence of different coke types on catalytic

View Article Online
DOI: 10.1039/D5GC02932E

reactions, provides a theoretical foundation for the design of coke-resistant catalysts. These efforts will contribute to the targeted development of high-performance catalysts that minimize the environmental impact of the conversion process and ultimately contribute to green chemistry and sustainable development.

Compared with the residual coke from biomass pyrolysis (termed "biochar" in this work), coke deposition refers to solid macromolecules[7] on catalyst surfaces or within pores formed from carbonaceous substances[8] in biomass pyrolysis volatiles, which block pore structures or cover active sites.[9] These deposits exhibit diverse compositions and complex structures.[10] Their physical morphology can be analyzed via electron microscopy, and the influence of the physical properties of coke on catalytic reforming reactions has been investigated[11]. However, elucidating the molecular-level structure of coke deposits and unraveling their formation mechanisms remains challenging. In related coke deposit studies, reactions with simple substrates such as dry reforming or propane dehydrogenation[12] are relatively straightforward to analyze. By contrast, real biomass pyrolysis volatile reforming faces greater complexity due to the diversity of intermediate products, making it difficult to identify key intermediates and pathways for coke formation.[13] Although studies have examined model biomass compounds, their catalytic conversion processes are very different from real biomass systems, offering limited practical guidance for industrial applications. Currently, researches primarily relies on the "hydrocarbon pool" theory to explain coke formation mechanisms.[14-16] According to the theory, during biomass pyrolysis, volatiles undergo deoxygenation over catalysts, generating unsaturated hydrocarbons that further condense into coke

View Article Online
DOI: 10.1039/D5GC02932E

deposits. Most studies based on this theory assume that coke is predominantly graphitic carbon[17] without further structural validation or mechanism-structure correlation. Furthermore, these works often focus solely on coke-forming reactions while neglecting the primary reforming reactions that produce fuel gases or light oils. This narrow focus fails to address the synergistic relationship within the overall reaction network.

To address these challenges, it is imperative to first elucidate the molecular structure of coke deposits. Previous studies have explored various characterization methods for coke deposits, primarily employing techniques such as infrared spectroscopy,[18] Raman spectroscopy,[10] and UV-visible spectroscopy[19] to directly analyze catalysts. However, these approaches are susceptible to interference from coexisting catalyst components. Alternatively, some methods involve extracting coke deposits from catalysts using harmful solvents (dichloromethane[14]) or corrosive agents (hydrofluoric acid[20]) before analysis, which inevitably generates environmentally hazardous waste. Moreover, spectroscopic techniques mainly focus on analyzing functional groups such as C-C, C-O, and C-H bonds. Consequently, the resulting data are typically interpreted based on a graphitic carbon framework with minor edge modifications (attached hydrocarbon or hydroxyl groups), failing to provide more detailed molecular-level information, particularly regarding the intrinsic structure of carbon layers.[14, 21] In recent years, Py-GC/MS has gained significant attention for the macromolecular characterization of polymers.[22, 23] This technique employs a fast pyrolysis furnace to heat samples under an inert atmosphere at high heating rates

View Article Online
DOI: 10.1039/D5GC02932E

(500 °C/min), and the resulting pyrolysis products are directly introduced into a gas chromatograph for separation, followed by mass spectrometry analysis. By qualitatively and quantitatively analyzing characteristic fragment ions produced during pyrolysis, the composition and structure of the original sample can be deduced. Py-GC/MS has been widely applied for structural analysis of organic polymers, including sludge[24] and plastics,[22] and has even been utilized to infer coal structures from fragment molecules.[25] Notably, despite coke deposits being carbon-rich macromolecular polymers, there have been scarcely any reports on the application of Py-GC/MS for characterizing their structural features on catalysts. Recognizing the technique's advantages in precise molecular structure analysis and its solvent-free pretreatment requirement for coke deposits, this study adopts Py-GC/MS to conduct a comprehensive investigation of the chemical structure of coke deposits. This approach not only circumvents the use of hazardous solvents but also enables direct molecular-level insights into coke formation mechanisms. The background to the study, other previous research approaches, and the research approach of this work are summarized in **Scheme 1**.

View Article Online
DOI: 10.1039/D5GC02932E

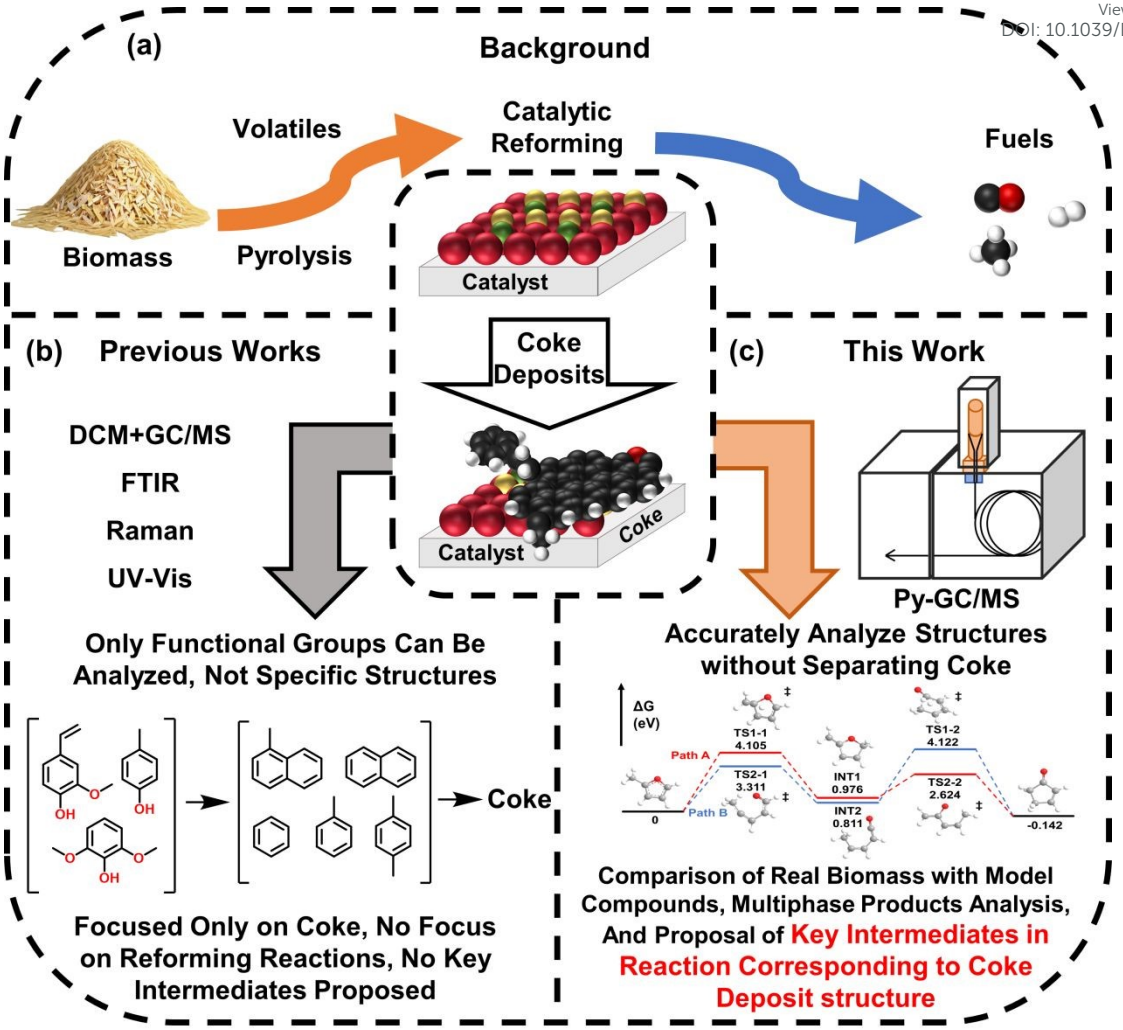

Scheme 1. Background to the study of coke deposits (a), other previous works (b), and this work (c).

To elucidate the mechanism of coke formation, it is essential to identify key intermediates and their evolution pathways. However, conventional fixed-bed reactor systems face significant challenges in capturing these transient intermediates during real biomass catalytic reforming processes. Py-GC/MS has emerged as a powerful analytical tool that not only enables structural characterization but also facilitates investigations into catalytic fast pyrolysis[26] and primary molecular analysis.[27] While this technique has been widely employed to decipher reaction pathways and identify intermediates in various chemical processes, conventional micro-scale Py-GC/MS

View Article Online
DOI: 10.1039/D5GC02932E

experiments fail to simultaneously study both the actual coke formation process and volatile reforming reactions.[27] In this work, we developed an innovative approach combining Py-GC/MS equipped with a micro quartz tube reactor for intermediate capture and fixed-bed ex-situ catalytic experiments for multiphase product collection. The catalytic reforming of wheat straw (WS) pyrolysis volatiles over Fe-Ni/Al_2O_3 catalysts for H_2-rich syngas production has been investigated using this integrated system (**Scheme 2**) and established comprehensive reaction pathways for coke deposit formation. Our results reveal, for the first time, the presence of five-membered ring structures in catalyst coke deposits and systematically examine their impact on catalytic performance. Furthermore, the role of the catalyst in the coke formation process was elucidated, and the behavior of coke deposition on different types of catalysts was experimentally verified by model compounds, and proposed a novel formation mechanism involving cyclopentenone as the key intermediate for five-membered ring structures in coke deposits. This provides a theoretical basis for understanding coke formation processes and their effects on reactions, as well as for constructing coke-resistant catalysts.

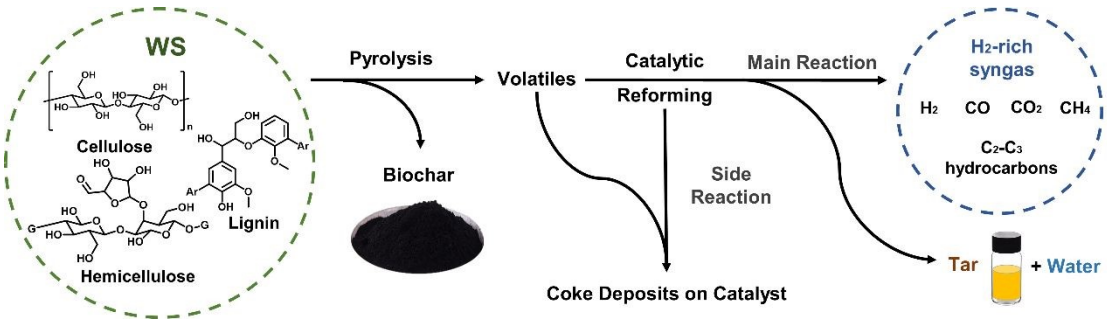

Scheme 2. The main and side reactions during the catalytic reforming of wheat straw pyrolysis volatiles.

View Article Online
DOI: 10.1039/D5GC02932E

2. Materials and methods

2.1 Materials

The biomass used in this study was wheat straw (WS) from rural areas of Sichuan Province, China. Detailed information regarding the processing procedures of WS and the selection of model compounds can be found in the **Supporting Information (SI)**. **Table S1** summarizes the proximate and final analyses of WS.

2.2 Catalyst preparation

The catalysts were synthesized by the precipitation-mixing method. Detailed synthesis procedures are provided in the **SI**.

2.3 Experimental

The fast pyrolysis experiments were conducted using a Py-GC/MS system, which consists of a micro-pyrolyzer (Frontier Lab, EGD/Py-3030D) and a gas chromatography-mass spectrometer (Shimadzu, GC-MS-QP2020 NX). The micro-pyrolyzer was equipped with a vertical microfurnace that was directly interfaced with the GC/MS separation inlet. As illustrated in **Fig. S1**, the experimental setup involved loading precisely weighed quantities of feedstock (8.0 ± 0.1 mg) and catalyst (4.0 ± 0.1 mg) into 70-mm-long micro quartz tubes with an internal diameter of 2 mm, separated by quartz wool packing. The pyrolysis protocol consisted of three sequential steps: (1) heating the micro-pyrolyzer to the predetermined reaction temperature, (2) rapidly introducing the micro-quartz tube into the pyrolysis zone for a precisely controlled

View Article Online
DOI: 10.1039/D5GC02932E

residence time of 60 s, and (3) immediately initiating the GC/MS analysis to characterize the volatiles generated through thermal decomposition.

The experimental procedure for fast pyrolysis of the model compounds was as same as above. The model compound was sampled as 10 ± 0.1 mg, in which cyclopentenone and cyclohexene were homogeneously mixed in a volume ratio of 1:1 before use.

The catalytic performance evaluation was performed in a custom-designed two-stage fixed-bed reactor system with an inner diameter of 50 mm, as schematically illustrated in **Fig. S2**. The reactor configuration consisted of two distinct zones: the left zone for feedstock placement (3.0 ± 0.1 g) and the right zone for catalyst loading (1.5 ± 0.05 g). Before initiating the reaction, the reactor system was purged with N_2 (99.99%) at a flow rate of 150 mL/min for 15 min to remove impurity gases. The gas flow rate was then adjusted to the standard reaction condition of 50 mL/min. The temperature program was carefully controlled using a multi-zone heating system. The catalyst zone (right section) was first heated to the target temperature at a controlled heating rate of 30 °C/min and stabilized for 20 min. Subsequently, the feedstock zone (left section) was heated to the desired temperature at a heating rate of 10 °C/min, followed by isothermal maintenance for the predetermined reaction duration.

The carbon mass in the gas phase was directly determined through gas chromatographic analysis and conversion. For other components, their carbon contents were measured by calcination at 800 °C in an air atmosphere using a tube furnace to convert carbon into carbon oxides, which were then collected and analyzed by gas

View Article Online
DOI: 10.1039/D5GC02932E

chromatography. The carbon-containing material to be calcined was placed in a quartz tube, with the outlet connected to a drying bottle and a gas bag. Anhydrous air was introduced at a flow rate of 50 mL/min, and the temperature was increased to 800 °C at a heating rate of 30 °C/min, followed by a 30 min holding time. By this time, the carbon-containing material had been completely oxidized and purged into the gas bag. The gas in the bag was analyzed by gas chromatography to determine the carbon mass. Details regarding gas chromatography calibration are provided in the **Supporting Information**. The carbon deposits in the reactor were determined by disassembling the reaction tube and placing it inside a larger tube for calcination. Both the biomass char (biochar) and the used catalyst were calcined directly. For tar analysis, after extraction with tetrahydrofuran, 1.5 g of column chromatography silica gel was added, followed by solvent removal through rotary evaporation, and then the silica gel adsorbed with tar was calcined. The carbon conversion rate and carbon balance, expressed as mass percentages, were obtained by dividing the carbon mass in each phase by the carbon mass in the dry biomass (calculated from ultimate analysis results).

2.4 Product analysis and catalyst characterizations

The biomass was loaded into a pre-weighed crucible (mass known) for pyrolysis. The combined mass of the crucible and biochar was measured post-reaction, with the char yield (Y_{char}) determined by mass difference. Tar products extracted by tetrahydrofuran were transferred to a pre-weighed round-bottom flask for rotary evaporation, with the tar yield (Y_{tar}) calculated by subtracting the flask's tare mass from

View Article Online
DOI: 10.1039/D5GC02932E

the total mass. All generated gases were treated as non-associating ideal gases under low partial pressures. Gas yields (Y_{gas}) were quantified via gas chromatography analysis combined with ideal gas law calculations based on measured volumes. Water yield (Y_{water}) was determined by the mass difference of drying bottles connected to the reactor outlet before and after experiments. Catalyst mass increase (Y_{coke})was measured by differential weighing of the catalyst-loaded crucible before and after the reaction. All mass measurements were performed on a precision analytical balance with 0.1 mg resolution (LC-FA1004, LICHEN). Product yields are reported as mass percentages relative to dry biomass feedstock, enabling complete mass balance closure. The reactor mass was monitored using a platform scale (precision ± 0.1 g), with no measurable mass changes detected during experiments. Therefore, reactor mass variations are not considered in the mass balance calculations. The yields calculated by mass fraction are as follows:

$$Y_{gas} = \frac{m_{gas}}{m_{WS}} \times (1)$$

$$Y_{tar} = \frac{m_{tar}}{m_{WS}} \times (2)$$

$$Y_{char} = \frac{m_{char}}{m_{WS}} \times (3)$$

$$Y_{water} = \frac{m_{water}}{m_{WS}} \times (4)$$

$$Y_{coke} = \frac{m_{used\ catalyst} - m_{fresh\ catalyst}}{m_{WS}} \times (5)$$

The gases generated from the reaction were collected using a gas bag and subsequently analyzed by gas chromatography (Agilent, 7980B). The gas yields by volume ($ml/g_{\text{-WS}}$) are calculated by dividing the individual volumes of each gas in the product by the raw material mass. After the reaction, the tar products deposited in both

View Article Online
DOI: 10.1039/D5GC02932E

the reactor tube and condensation flask were extracted using tetrahydrofuran (THF). The solvent was subsequently removed by rotary evaporation before GC/MS (Shimadzu, GC-MS-QP2020, NX) analysis. THF was selected as the extraction solvent due to its lower environmental hazard compared to conventional tar-collecting solvents such as n-hexane.[28] Importantly, the recovered THF after rotary evaporation can be recycled for subsequent extractions, thereby minimizing waste generation and environmental impact. After the reaction, the catalyst was transferred to a measuring cup and cracked by Py-GC/MS at a temperature of 100 °C above the reaction temperature. This process allowed for the analysis of the surface functional groups.

The characterization details are provided in the **SI**.

3. Results and discussion

3.1 Fast pyrolysis of WS in Py-GC/MS

Fig. 1-2 illustrates the distribution of volatile compounds generated by catalytic fast pyrolysis of WS, as well as fragment molecules produced by pyrolysis of used catalysts. Detailed structures of representative substances in each category are provided in the **SI**. **Fig. 1(a)** shows the volatiles produced by the catalytic pyrolysis of WS over 5Fe-0.8Ni/Al_2O_3 at different temperatures, and the corresponding chromatograms are shown in **Fig. S7(a)**. Subsequently, the used catalyst was subjected to Py-GC/MS analysis to examine the coke deposits, and the results are presented in **Fig. 1(b)**. The composition of coke deposits can be characterized by the H/C ratio,[29] where a higher ratio indicates “softer” coke, while a lower ratio suggests “harder” coke. It is widely

View Article Online
DOI: 10.1039/D5GC02932E

accepted that “hard” coke deposits are the primary cause of catalyst deactivation. The pyrolysis of coke deposits predominantly yields aliphatic hydrocarbons, indicating that “soft” coke is formed during fast pyrolysis experiments. This represents the initially formed coke deposits. As the temperature increases, the catalyst promotes the cracking of oxygen-containing structures[30] in the volatiles, thereby reducing the oxygen content in the coke deposits and increasing the proportion of aromatic carbon structures, and the coke gradually becomes “harder”. The increased proportion of aliphatic hydrocarbons at 800 °C may be attributed to the formation of graphitized units in the coke deposits under high-temperature conditions,[31] which resist further cracking. Notably, aromatic hydrocarbons with five-membered ring structures, such as indene and its derivatives, were detected in the coke deposits, and their content decreased with increasing temperature. These loosely packed structures inherently contain aliphatic moieties such as methylene groups, suggesting that “soft” coke deposits consist not only of aliphatic and oxygen-containing functional groups but also five-membered ring structures. Similar compounds were observed in the volatiles, and their structural resemblance to “soft” coke deposits indicates that they serve as precursors for coke formation. The reactive double bonds[32] in indene, connected to aromatic rings, undergo polymerization under catalytic action to form fluorene. Compared with non-catalytic experiments (**Table 4**), the presence of the catalyst enhances the conversion of oxygenated compounds and the formation of aromatic hydrocarbons while simultaneously catalyzing coke deposition. The results of experiments using 5Fe-0.8Ni/A-Al_2O_3 at different temperatures are shown in **Fig. 2(a-b)**, with the

View Article Online
DOI: 10.1039/D5GC02932E

corresponding chromatograms in **Fig. S7(b)**. This catalyst exhibits remarkable catalytic deoxygenation and polymerization capabilities at high temperatures, whereas at lower temperatures, it tends to form oxygen-containing coke deposits, a consequence of the support's varying adsorption capacity for volatiles.[33] The coke deposits on this catalyst exhibit a higher H/C ratio, indicating "softer" coke. The increased proportion of indene in the aromatic hydrocarbons derived from coke deposit pyrolysis underscores the significance of five-membered ring structures in defining the characteristics of "soft" coke. The volatiles in coke deposits, along with oxygenated compounds, aliphatic hydrocarbons, and aromatic hydrocarbons, exhibit parallel trends after rapid interactions, suggesting that coke deposits primarily originate from adsorbed but not promptly desorbed volatiles.

View Article Online
DOI: 10.1039/D5GC02932E

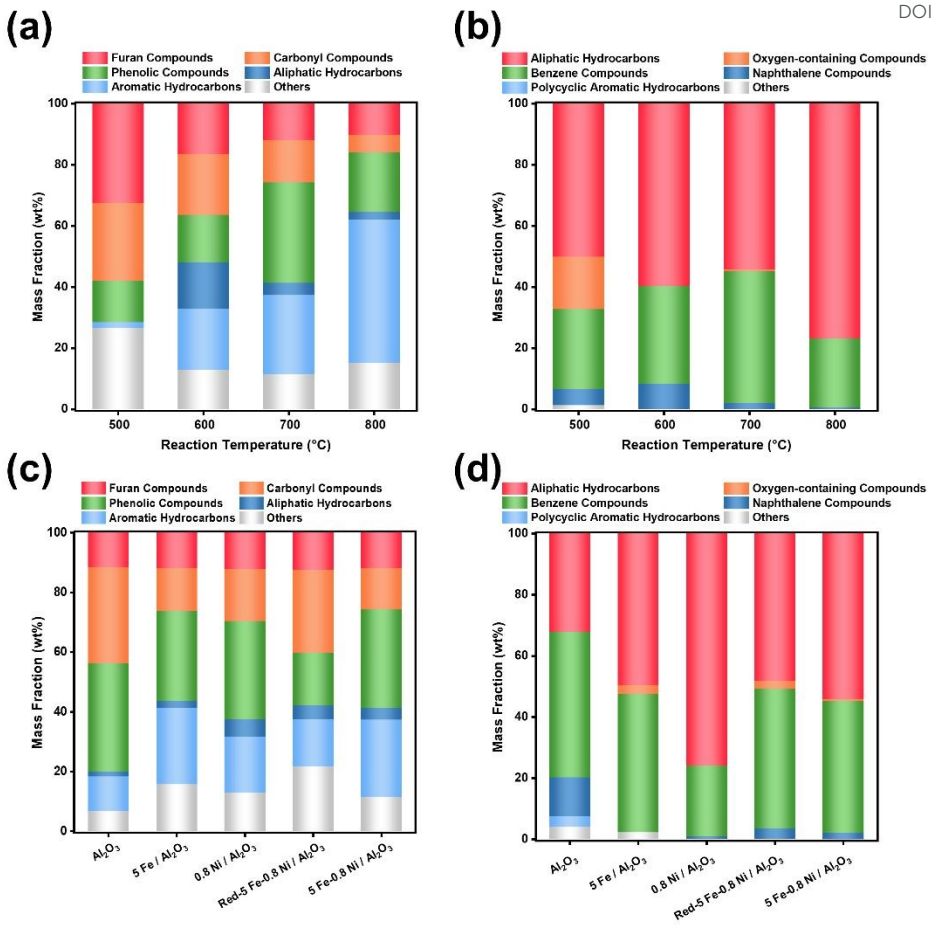

Fig. 1. In experiments using Al_2O_3 as a catalyst support, volatiles (a and c) produced from the catalytic fast pyrolysis experiments of WS in Py-GC/MS, and the results of catalyst coke accumulation detected by Py-GC/MS of the used catalysts (b and d).

To elucidate the roles of individual metal components and supports in the catalytic conversion of volatiles, single-metal catalysts (5Fe/Al_2O_3, 0.8Ni/Al_2O_3, 5Fe/A-Al_2O_3, and 0.8Ni/A-Al_2O_3), pre-reduced catalysts (Red-5Fe-0.8Ni/Al_2O_3 and Red-5Fe-0.8Ni/A-Al_2O_3), and bare supports (Al_2O_3 and A-Al_2O_3) were employed in fast pyrolysis experiments at 700 °C. The results are presented in **Fig. 1(c-d)** and **Fig. 2(c-d)**. The pre-reduced catalysts yielded a higher proportion of carbonyl compounds, suggesting that pre-reduced catalysts suppress the further conversion of aldehydes and ketones. Notably, no indene was detected in the products, likely because carbon-

View Article Online
DOI: 10.1039/D5GC02932E

containing species preferentially reduced the metal oxides.[34] The pyrolysis of coke deposits from these catalysts produced a higher fraction of aromatic hydrocarbons, indicating that pre-reduction promotes the formation of "hard" coke. For single-metal catalysts, volatile analysis revealed distinct roles for each metal: Fe facilitates the deoxygenation of oxygenated compounds,[35] while Ni promotes the dehydrogenation of hydrocarbons.[7] Compared with bimetallic catalysts, coke deposits on single-metal catalysts exhibited more aromatic ring structures and fewer five-membered ring structures, suggesting "harder" coke. This may explain why single-metal catalysts are more prone to deactivation. The findings also imply that bimetallic catalysts form new active phases with enhanced resistance to coke deposition. The supports significantly influence catalytic conversion by providing additional collision sites for radical reactions. Analysis of the supports revealed that while they do not enhance dehydrogenation or deoxygenation of volatiles,[36] they promote the enrichment of highly unsaturated molecules, leading to the formation of "harder" coke. Comparing Al_2O_3 and A-Al_2O_3, the latter possesses a more polar surface structure,[37] which reduces its ability to enrich weakly polar aromatic hydrocarbons but enhances its affinity for strongly polar compounds (oxygen-containing species). Consequently, coke deposits on A-Al_2O_3 contained more five-membered ring structures than those on metal-loaded catalysts, suggesting that polar supports favor the formation of such structures.

View Article Online
DOI: 10.1039/D5GC02932E

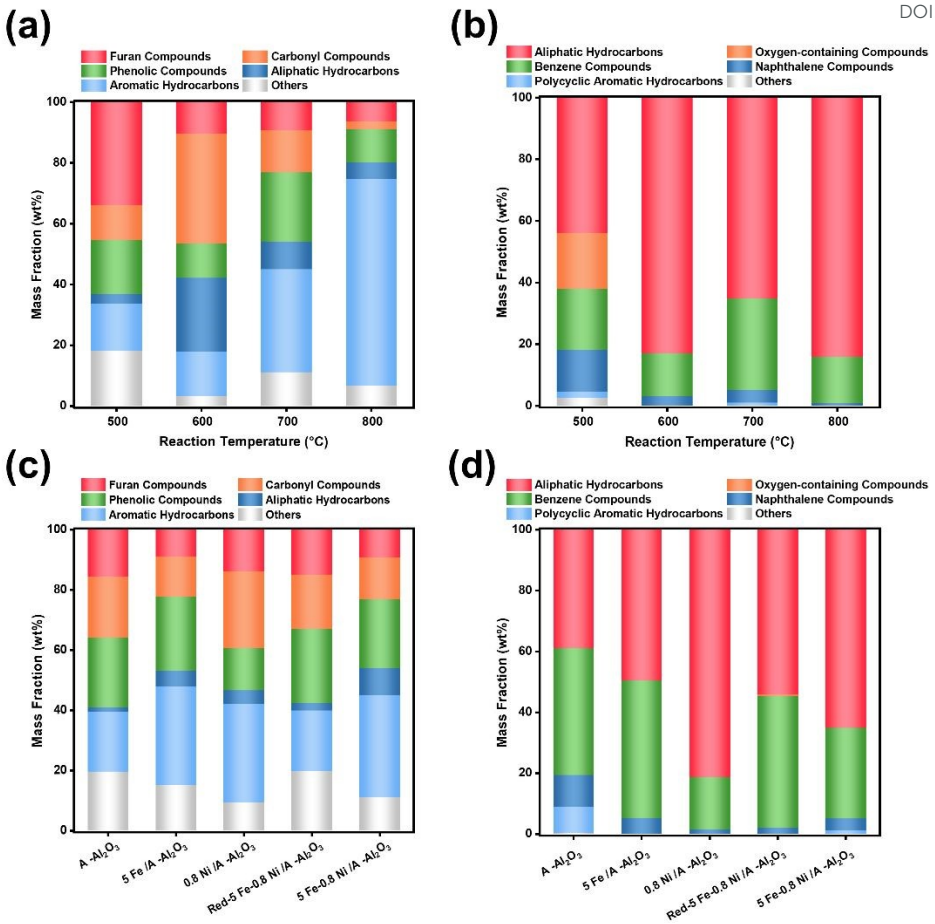

Fig. 2. In experiments using A-Al_2O_3 as a catalyst support, volatiles (a and c) produced from the catalytic fast pyrolysis experiments of WS in Py-GC/MS, and the results of catalyst coke accumulation detected by Py-GC/MS of the used catalysts (b and d).

3.2 Fixed-bed scaled-up experiments of WS and catalysts characterization

To investigate the formation process of real coke deposits, scaled-up experiments with a holding time of 30 min were conducted in the fixed-bed reactor **(Fig.S2**). As shown in **Fig. 3(a-c),** the gases, condensed volatiles, and used catalysts obtained from experiments at different temperatures using 5Fe-0.8Ni/Al_2O_3 were analyzed. The chromatogram obtained by analyzing the coke accumulation is shown in **Fig. S8(a)**. The yields of various phase products and the corresponding mass balance were

View Article Online
DOI: 10.1039/D5GC02932E

summarized in **Table S2**. At lower temperatures, the catalyst activity was not fully utilized, making it more difficult to fully crack the volatiles, resulting in lower gas yields[38] and higher tar yields, which are undesirable products. The higher CO_2 yield at these temperatures suggests that decarboxylation is more prevalent compared to decarbonylation and dehydrogenation reactions. As the temperature increases beyond 700 °C, the H_2 yield rises sharply due to the higher bond energy of C-H bonds. In contrast, the decarbonylation reaction, which produces CO, proceeds more completely at 700 °C. Comparison with micro-quartz tube fast pyrolysis experiments reveals that increasing the temperature and prolonging the holding time have similar effects on the conversion of volatiles. In the scaled-up experiments, biomass components such as cellulose, hemicellulose, and lignin were sufficiently cracked at 500 °C to produce volatiles, primarily phenols, aliphatic hydrocarbons, and carboxylic acids. Notably, some phenolic compounds were formed through the collision of furan molecules in the volatiles rather than through catalytic action.[39] The increase in aromatic hydrocarbons content and the number of rings in polycyclic compounds with rising temperature indicate that the catalyst promotes dehydrocyclization. Five-membered ring compounds, such as fluorene, were identified in the condensation fraction, while indene was detected in the pyrolysis products of the used catalysts. These findings confirm that the low-unsaturated structures in "soft" coke deposits include not only branched chains such as aliphatic hydrocarbon groups, as previously reported in the literature, but also five-membered rings at the edges of aromatic carbon layers. The transition of coke deposits from "soft" to "hard" with increasing temperature was further evidenced by

View Article Online
DOI: 10.1039/D5GC02932E

the decrease in aliphatic hydrocarbons and indene compounds produced during high-temperature pyrolysis (500-700 °C) of the used catalyst as the operating temperature rose. The five-membered ring structures in coke deposits may form through the enrichment of polycyclic compounds with five-membered rings in the volatiles on the catalyst,[16] as evidenced by the changing patterns of compound content in **Fig. 2**. Thermodynamically, the cyclization of chain compounds to form five-membered rings is highly favorable,[40] and these structures may also arise from the dehydrocyclization of aliphatic groups enriched on the catalyst surface. The aromatic hydrocarbons produced from the pyrolysis of coke deposits can be categorized into two types: unsubstituted aromatics and branched aromatics. Unsubstituted aromatics arise from the pyrolysis of graphite carbon edges without branched chains, whereas branched aromatics result from carbon layers with branched edges and lower regularity, characteristic of "soft" coke formation. At higher temperatures, substituents (mainly methyl, ethyl, and vinyl groups) decrease due to chain scission, leading to a reduction in branched aromatics and the formation of "hard" coke. Additionally, the presence of small amounts of biphenyl and styrene suggests that the surface of coke deposits may also feature aromatic groups, such as phenyl groups, rather than solely aliphatic moieties. These structures collectively constitute "soft" coke deposits.

View Article Online
DOI: 10.1039/D5GC02932E

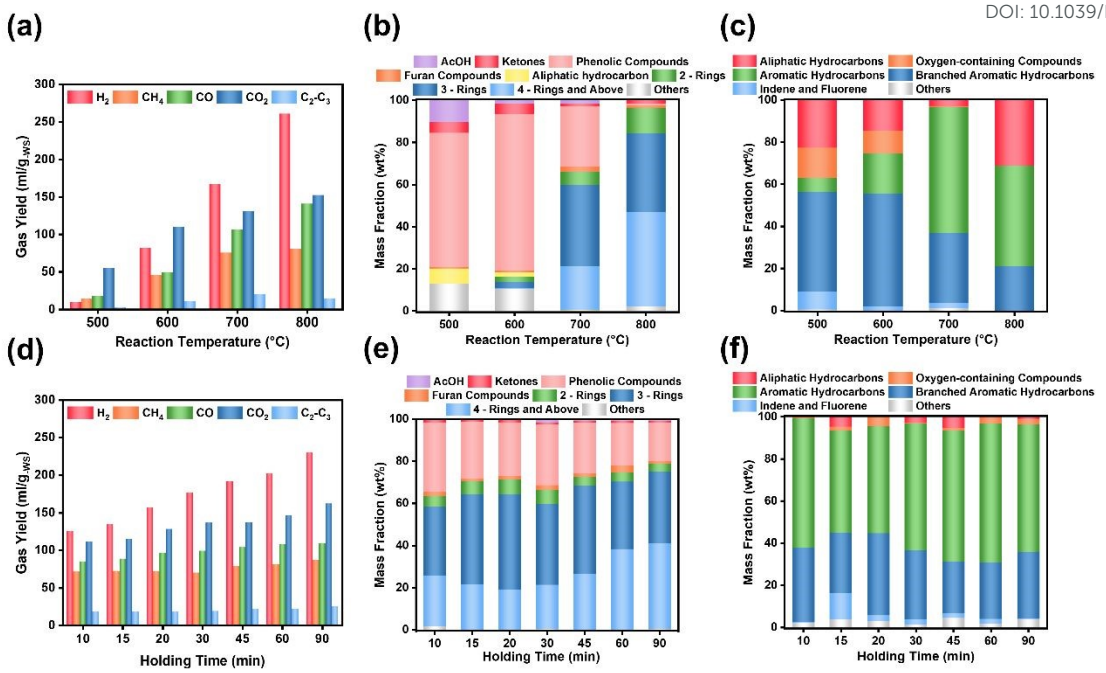

Fig. 3. In experiments using 5Fe-0.8Ni/Al_2O_3 as the catalyst, gas products (a and d). condensable fractions (b and e), and results of used-catalyst detection by Py-GC/MS for the catalyst after use (c and f), obtained by ex-situ catalytic pyrolysis of WS for volatiles reforming in the fixed-bed reactor.

Experiments without a catalyst were conducted at 700 °C, and the results are presented in **Fig. S9**. Extending the holding time led to a decrease in phenolic content and a significant increase in acetic acid content, which is attributed to the decomposition of phenols containing acetoxy groups. Additionally, the aromatic hydrocarbon content exhibited only a marginal increase, indicating that the catalyst plays a crucial role in promoting the decarboxylation and decarbonylation reactions of oxygenated compounds. While the catalyst facilitates cracking reactions that produce H_2, CO, and other small gaseous molecules, it also catalyzes polymerization reactions that form polycyclic aromatic hydrocarbons (PAHs), which serve as precursors for coke deposits. However, in non-catalytic experiments, the proportion of fluorene in the

View Article Online
DOI: 10.1039/D5GC02932E

produced aromatic hydrocarbons was relatively low, suggesting that the catalyst enhances the formation of five-membered ring structures.

Experiments were conducted in the fixed-bed reactor using the 5Fe-0.8Ni/Al_2O_3 catalyst with varying holding times at 700 °C. As shown in **Fig. 3(d-f)**, the gases, condensed volatiles, and used catalysts were analyzed. The yields of CH_4 and C_2-C_3 hydrocarbons remained relatively stable with increasing holding time and were higher than those in non-catalytic experiments. This suggests that the organic precursors of these molecules were limited, while the reactions leading to coke deposits were associated with the formation of inorganic molecules such as H_2, CO, and CO_2. The yields of various phase products and the corresponding mass balance were summarized in **Table S4**. The tar yield decreased with prolonged holding time, as the tar was converted into non-condensable gases and coke deposits on the catalyst. During the reaction, phenolic compounds are converted into aromatic hydrocarbons through CO removal, while hydrocarbons undergo catalytic polymerization and dehydrogenation to form aromatics. The number of aromatic rings increases with prolonged holding time, leading to higher molecular weights and lower saturated vapor pressures, which facilitate the transformation of these substances into coke deposits.[16] The increase in carboxylic acid content with holding time further indicates that the formation of coke deposits encapsulates the catalyst, reducing its ability to convert small molecules. As the holding time increased, the content of indene compounds and branched aromatics in the pyrolysis products of the coke deposits on the catalyst decreased, suggesting that "soft" coke deposits on the catalyst spontaneously transformed into "hard" coke. This

View Article Online
DOI: 10.1039/D5GC02932E

transformation involves the cyclization and dehydrogenation of edge aliphatic groups, forming more ordered cyclic structures that are more likely to encapsulate the catalyst and cause deactivation.

Experiments were conducted on each type of catalyst using Al_2O_3 as the support at 700 °C with a holding time of 30 min. As shown in **Fig. 4(a-c)**, the gases, condensed volatiles, and used catalysts were analyzed. The yields of various phase products and the corresponding mass balance were summarized in **Table S6**. The thermogravimetric analysis (TGA) was performed to determine the weight loss rate of the catalysts after each use, and the amount of coke accumulation is presented in **Table 1**. The pre-reduced catalysts exhibited greater catalytic ability for phenols deoxygenation and hydrocarbons dehydrocyclization, likely due to the exposure of more metal sites. The amount of coke deposits on the pre-reduced catalyst was relatively large, but there were fewer five-membered ring structures in the coke deposits. The distribution of gas products revealed that, in the actual catalytic process, metal oxides in the fresh catalyst are primarily reduced by carbon-containing components in the volatile fraction rather than by H_2. The interaction between metal oxides and carbon-containing species may generate more irregular carbonaceous intermediates, which act as "triggers" for coke deposit growth, resulting in a distinct coke deposit structure compared to that of pre-reduced catalysts. Single-metal catalysts produced more coke deposits than bimetallic catalysts, with Ni-based catalysts being particularly prone to higher coke accumulation. The higher content of aliphatic hydrocarbons cracked from these coke deposits suggests that the coke structure transitions from "hard" at the core to "soft" at the surface. Al_2O_3

View Article Online
DOI: 10.1039/D5GC02932E

also exhibits catalytic activity in reforming biomass pyrolysis volatiles, leading to coke deposit formation on the support surface. TGA further indicated that the transformation of "soft" coke to "hard" coke involves the removal of small molecules. Polymerization and cracking occur simultaneously during coke deposit formation, with "harder" coke deposits being lighter in weight. The tar yield correlated well with TGA results, confirming that volatiles form coke deposits by eliminating small gaseous molecules while increasing their unsaturation. Combining the results from experiments with different holding times, it can be concluded that hydrogen-producing reactions play a major role in coke deposit formation.

Table 1. TGA in the air atmosphere of used catalysts.

Used-Catalyst	weight loss rate (%)	Used-Catalyst	weight loss rate (%)
5Fe-0.8Ni/Al_2O_3	3.12	5Fe-0.8Ni/A-Al_2O_3	3.82
Red-5Fe-0.8Ni/Al_2O_3	3.86	Red-5Fe-0.8Ni/A-Al_2O_3	4.65
5Fe/Al_2O_3	3.15	5Fe/A-Al_2O_3	3.96
0.8Ni/Al_2O_3	4.39	0.8Ni/A-Al_2O_3	5.00
Al_2O_3	4.22	A-Al_2O_3	4.44
5Fe-0.8Ni/SiO_2	2.98	ZSM-5	5.35

View Article Online
DOI: 10.1039/D5GC02932E

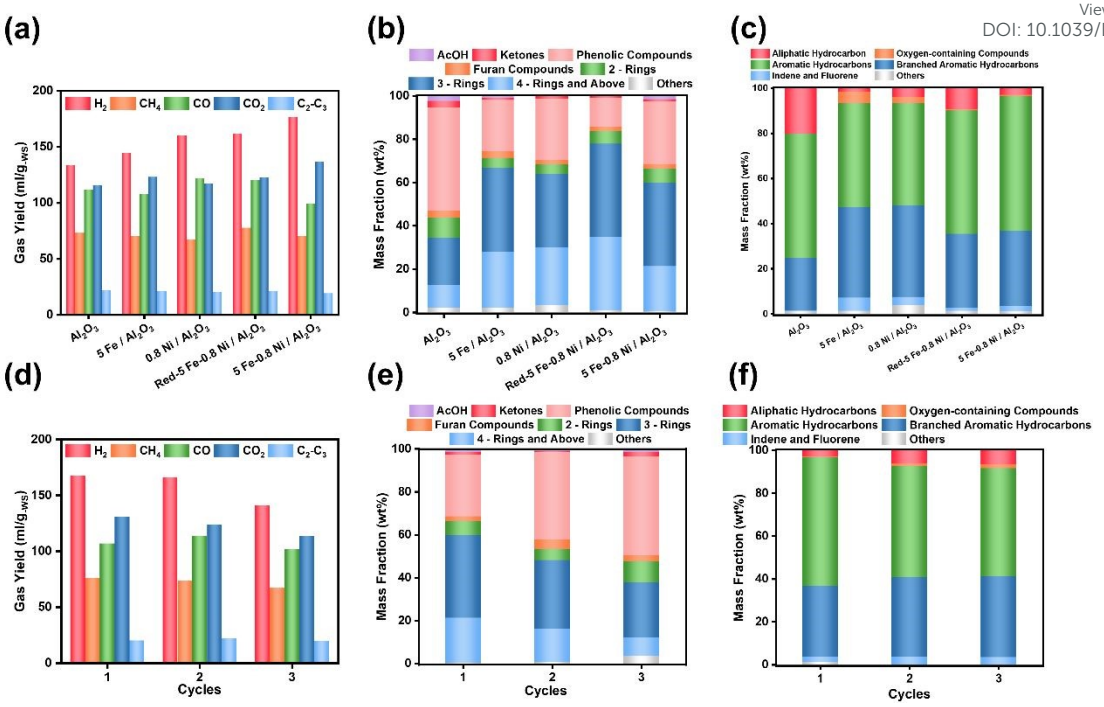

Fig. 4. Gas products (a and d). condensable fractions (b and e), and results of used-catalyst detection by Py-GC/MS for the catalyst after use (c and f), obtained by ex-situ catalytic pyrolysis of WS for volatiles reforming in the fixed-bed reactor.

To further investigate the influence of pre-formed coke deposition on subsequent H_2 production and coke deposition, three consecutive recycling experiments were conducted using 5Fe-0.8Ni/Al_2O_3. As shown in **Fig. 4(d-f),** the gases, condensed volatiles, and used catalysts were analyzed. The yields of various phase products and the corresponding mass balance are summarized in **Table S7**. The gas production decreased significantly after the third cycle, indicating that the coke deposits had either encapsulated the active sites or blocked the pores. The increase in CO production may result from the interaction of volatiles with the coke deposits.[41] The conversion of phenolic compounds to aromatic and polycyclic hydrocarbons progressively decreased with each cycle, suggesting a gradual decline in the catalyst's dehydrogenation capability. The pyrolysis products of the used catalyst from the second cycle were

View Article Online
DOI: 10.1039/D5GC02932E

similar in composition to those from the third cycle, suggesting that the coke deposit structure stabilized after two cycles. This stabilization indicates that the surface of the initially deposited coke becomes enriched with low-unsaturated and oxygenated substances.[14] However, as active sites became encapsulated, these species could not undergo further transformation, and five-membered ring structures ceased to form, ultimately leading to "hard" coke deposition and catalyst deactivation. These findings demonstrate that while the catalyst's active sites promote coke deposition, they are simultaneously inhibited by the accumulating deposits. The tar yield increased with cycle number, creating a vicious cycle: the catalyst facilitates coke formation while performing its function, but the accumulating coke deposits progressively suppress its efficacy.

Parallel experiments were also conducted using 5Fe-0.8Ni/A-Al_2O_3. As shown in **Fig. 5(a-c)**, the gases, condensed volatiles, and used catalysts obtained from reactions at different temperatures were analyzed. The yields of various phase products and the corresponding mass balance were summarized in **Table S3**. The chromatogram of the coke accumulation is shown in **Fig. S8(b)**. A-Al_2O_3, characterized by a larger specific surface area and stronger acidity **(Fig. 8, Table 3)**, effectively adsorbs volatiles, resulting in higher gas yields compared to catalysts with Al_2O_3 as the support. As the temperature increased, phenolic compounds were progressively converted to benzofurans. The benzofuran content exceeded that observed in experiments with 5Fe-0.8Ni/Al_2O_3, indicating that the A-Al_2O_3 support inhibits the deoxygenation of furan compounds to form aromatics. This is further supported by the lower CO yields in these

View Article Online
DOI: 10.1039/D5GC02932E

experiments. The pyrolysis of used catalysts revealed a significantly higher proportion of five-membered ring structures accompanied by aliphatic hydrocarbons, indicating that the A-Al_2O_3 support plays a guiding role in the formation of "soft" coke. The observed reduction in tar yield compared to 5Fe-0.8Ni/Al_2O_3 systems suggests that controlled formation of "soft" coke deposits positively influences tar conversion efficiency.

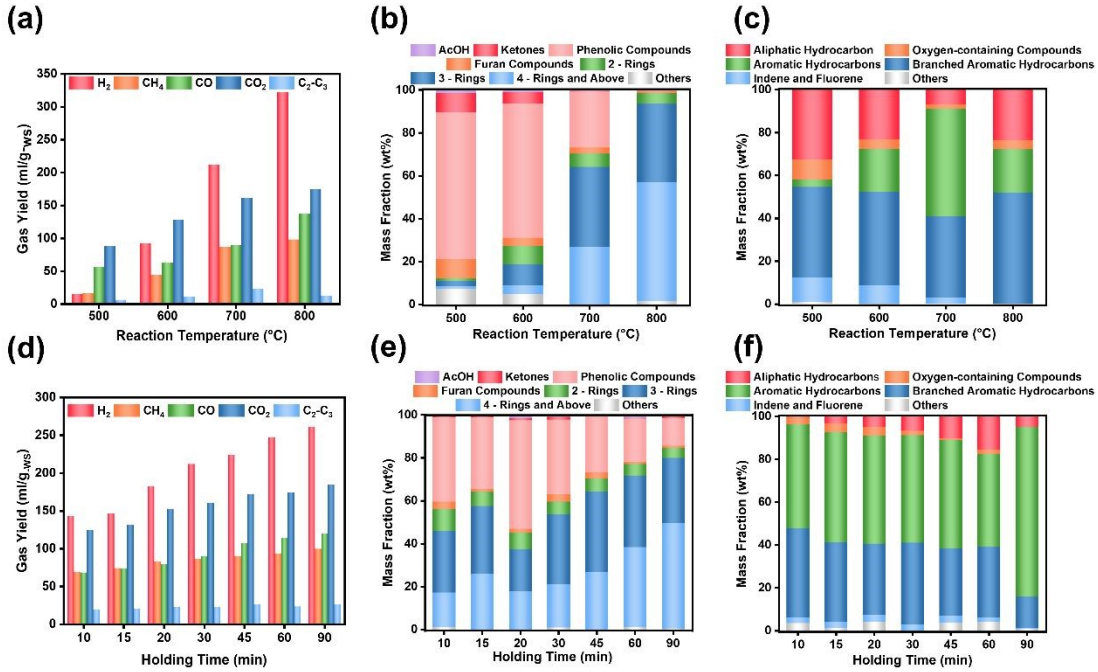

Fig. 5. In experiments using 5Fe-0.8Ni/A-Al_2O_3 as the catalyst, gas products (a and d). condensable fractions (b and e), and results of used-catalyst detection by Py-GC/MS for the catalyst after use (c and f), obtained by ex-situ catalytic pyrolysis of WS for volatiles reforming in the fixed-bed reactor.

Experiments were conducted at 700 °C using 5Fe-0.8Ni/Al_2O_3 with varying holding times. As shown in **Fig. 5(d-f)**, the gases, condensed volatiles, and used catalysts were analyzed. The yields of various phase products and the corresponding mass balance were summarized in **Table S5.** The phenolic compounds exhibited an

View Article Online
DOI: 10.1039/D5GC02932E

initial increase followed by a decrease, likely due to the polar nature of acidic sites stabilizing polar compounds.[42] These compounds accumulated to a certain extent before initiating catalytic reactions at the metal sites, while other compounds reacted preferentially in the early stages. In contrast, 5Fe-0.8Ni/A-Al_2O_3 demonstrated superior catalytic conversion of oxygenated compounds, significantly transforming phenolic compounds into benzofurans, which were also detected in the pyrolysis products of used catalysts. The more polar A-Al_2O_3 support tends to adsorb polar substances more effectively, resulting in less regular formation of coke deposits on its surface. TGA revealed that the amount of coke deposits on the A-Al_2O_3 was significantly higher than that on the 5Fe-0.8Ni/Al_2O_3. As the holding time increased, there was a notable enrichment of low-unsaturation functional groups on the coke deposits, indicating that the A-Al_2O_3 support inhibits the conversion of aliphatic radicals. Unlike 5Fe-0.8Ni/Al_2O_3, the 5Fe-0.8Ni/A-Al_2O_3 system maintained considerable tar conversion efficiency even with extended holding times. This observation suggests that "soft" coke deposits containing five-membered ring structures do not primarily contribute to catalyst deactivation.

Experiments were conducted on each type of catalyst using A-Al_2O_3 as the support at 700 °C with a holding time of 30 min. As shown in **Fig. 6(a-c)**, the resulting gases, condensed volatiles, and used catalysts were analyzed. The yields of various phase products and the corresponding mass balance were summarized in **Table S6**. The amount of coke deposits on catalysts with A-Al_2O_3 was consistently higher than that on catalysts with Al_2O_3. However, the difference in coke deposit accumulation for a single

View Article Online
DOI: 10.1039/D5GC02932E

support was minimal. The variation in coke deposit accumulation after metal loading can be attributed to differences in the distribution of metal sites and active phases, which vary with the support (**Fig. 8**). The pattern of change in different metal site types was similar to that observed with Al_2O_3 supports. However, A-Al_2O_3, due to its inherent acidic sites, catalyzes the coking of aromatics, resulting in higher PAHs[43]. Despite this, the cyclization of adsorbed substances is inhibited, preventing excessive growth of aromatic carbon lamellae. Consequently, the coke deposits formed are predominantly "soft" coke.

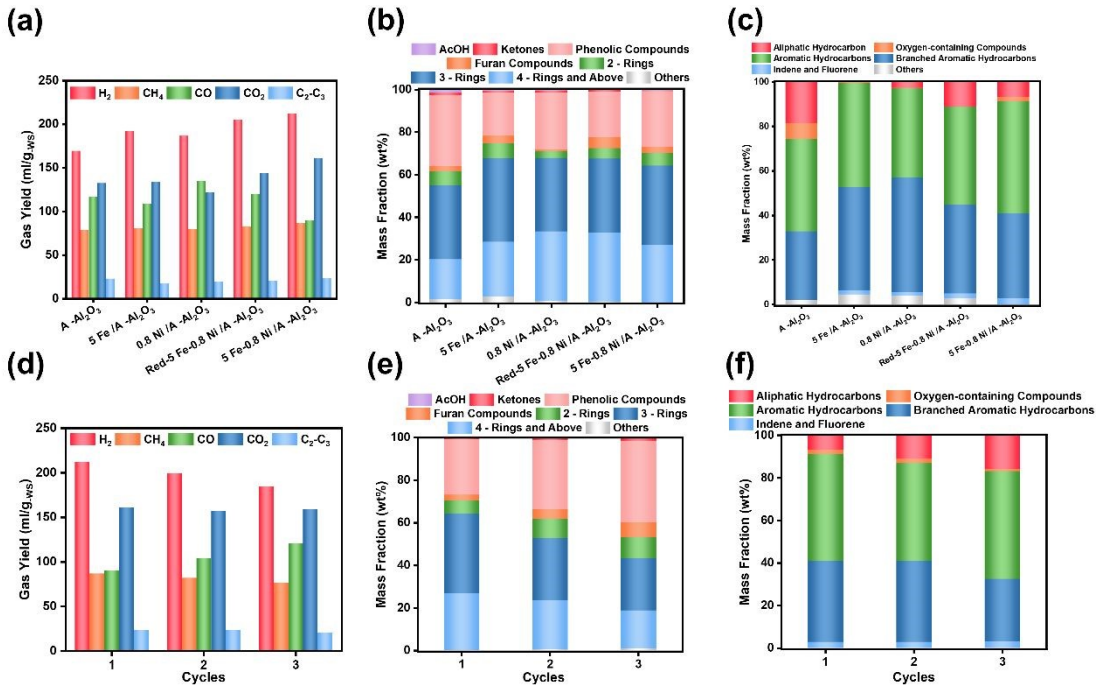

Fig. 6. Gas products (a and d). condensable fractions (b and e), and results of used-catalyst detection by Py-GC/MS for the catalyst after use (c and f), obtained by ex-situ catalytic pyrolysis of WS for volatiles reforming in the fixed-bed reactor.

Three-cycle experiments were conducted using 5Fe-0.8Ni/A-Al_2O_3. As shown in **Fig. 6(d-e)**, the gases, condensed volatiles, and used catalysts were analyzed. The yields of various phase products and the corresponding mass balance were summarized in

View Article Online
DOI: 10.1039/D5GC02932E

Table S8. The gas yield remained stable across all three cycles, indicating that the formation of "soft" coke had a less significant impact on the key active sites compared to 5Fe-0.8Ni/Al_2O_3. As the number of cycles increased, the catalyst's ability to convert oxygenated compounds into aromatics diminished. However, the distribution of compounds from the pyrolysis of the used catalysts did not stabilize. The content of aliphatic hydrocarbons continued to rise, while the content of five-membered ring structures decreased. This suggests that the structural order of the coke deposit surface continued to decrease, influenced by the nature of the support.

The experiments involving the catalytic reforming of WS at 700 °C over 5Fe-0.8Ni/Al_2O_3 and 5Fe-0.8Ni/A-Al_2O_3 for 30 min were conducted to evaluate the carbon conversion and carbon balance of the two catalytic systems, as summarized in **Table 2**. Compared with 5Fe-0.8Ni/Al_2O_3, 5Fe-0.8Ni/A-Al_2O_3 reduced the carbon content in gaseous products by promoting carbon fixation in the form of coke deposits, thereby suppressing carbon oxide emissions. The lower tar yield and higher carbon conversion observed with 5Fe-0.8Ni/A-Al_2O_3 can be attributed to the enhanced polymerization and higher carbon content of the tar reformed over this catalyst. Interestingly, the carbon content of biochar was also lower, likely because 5Fe-0.8Ni/A-Al_2O_3 more readily reacted with volatiles, thereby reducing secondary reactions of primary volatiles and primary biochar to some extent.[44]

Table 2. Carbon conversion and carbon balance for each product of the biomass pyrolysis volatiles catalytic reforming, in mass per cent (wt.%).

Catalysts	Biochar	Tar	Gas	Coke deposits on the catalyst	Coke deposits in the reactor	Carbon balance
5Fe-0.8Ni/Al_2O_3	51.2	16.8	22.8	5.1	1.4	97.3
5Fe-0.8Ni/A- Al_2O_3	50.5	17.1	20.9	7.4	1.8	97.7

As shown in **Fig. 7(a)**, Raman spectroscopy was employed to analyze the coke deposits on the catalysts. The D band was observed at approximately 1329 cm^{-1}, while the G band appeared at around 1604 cm^{-1}. The degree of structural disorder in the coke deposits was evaluated using the intensity ratio of the D band to the G band (I_D/I_G). It was found that this ratio exhibited a perfect positive correlation with the proportion of aromatic hydrocarbons containing five-membered rings, as determined by Py-GC/MS analysis of the coke deposits. This result indicates that the five-membered ring structures within the coke deposits can be regarded as representative features of less ordered "soft" coke. Moreover, these findings demonstrate that Py-GC/MS is a scientifically robust and feasible method for the characterization and analysis of coke deposits. A Comprehensive analysis of all experiments shows that A-Al_2O_3-supported catalysts direct the formation of "soft" coke with five-membered ring structures, thereby enhancing deactivation resistance.

View Article Online
DOI: 10.1039/D5GC02932E

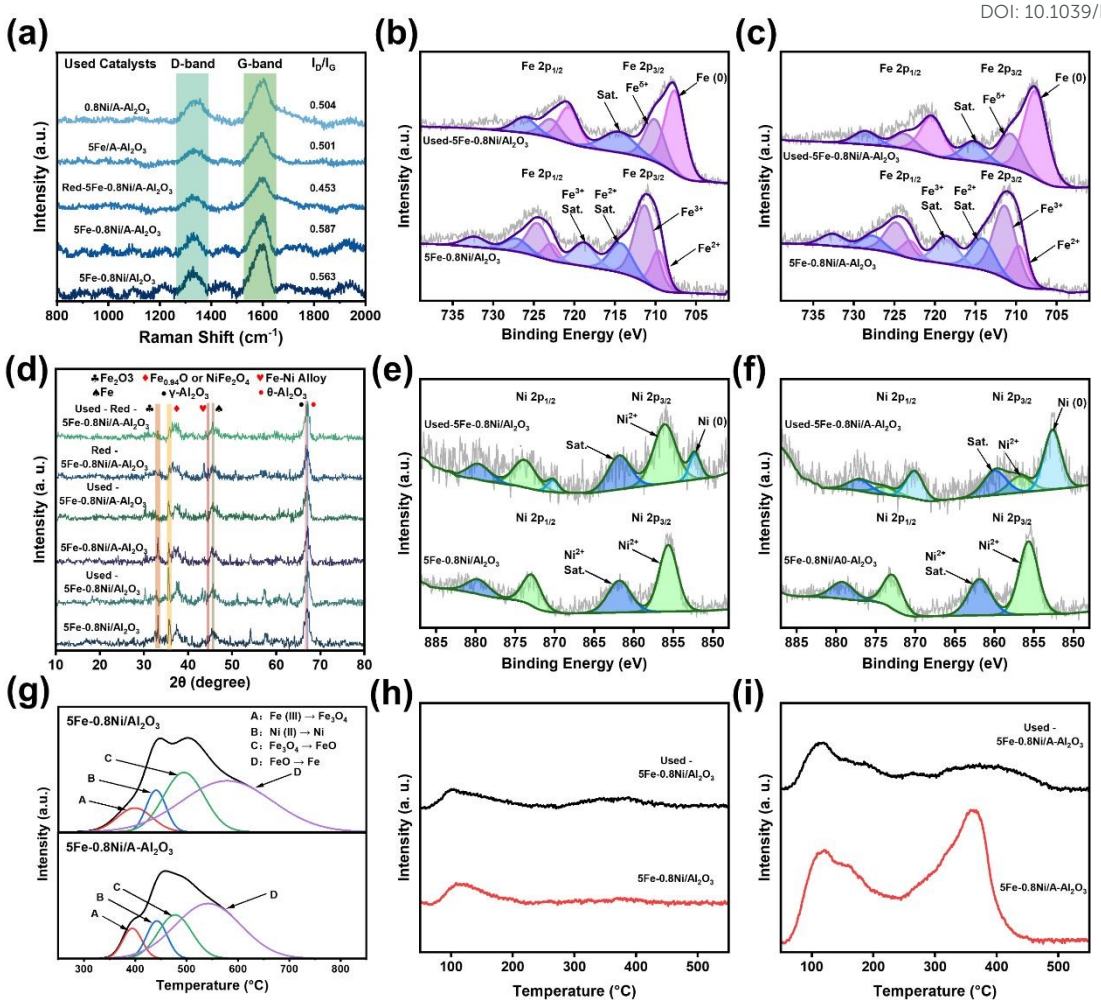

Fig. 7. Raman spectroscopic characterization of used catalysts (a). Fe 2p XPS spectra of fresh/used catalysts (b-c). XRD images of fresh/used catalysts (d). Ni 2p XPS spectra of fresh/used catalysts (e-f). H_2-TPD curves of 5Fe-0.8Ni/Al_2O_3 and 5Fe-0.8Ni/A-Al_2O_3 (g). NH_3-TPD curves of fresh/used 5Fe-0.8Ni/Al_2O_3 (h). NH_3-TPD curves of fresh/used 5Fe-0.8Ni/Al_2O_3 (i).

The fresh and used 5Fe-0.8Ni/Al_2O_3, 5Fe-0.8Ni/A-Al_2O_3, and Red-5Fe-0.8Ni/A-Al_2O_3 catalysts were analyzed by XRD, and the results are presented in **Fig. 7(d)**. The crystalline type of Al_2O_3 is θ-type (PDF # 04-0800) corresponding to the P group, whereas A-Al_2O_3 is γ-type (PDF # 10-0425) corresponding to the F group. The γ-type transforms into the θ-type after use, indicating that the interaction of volatiles with the

View Article Online
DOI: 10.1039/D5GC02932E

catalysts accelerates the transformation of the support's crystal type. The structural differences in the coke deposits produced by each catalyst may be influenced not only by the specific surface area resulting from the crystal type but also by the acidic sites (surface polarity).[42] In fresh catalysts, the metals exist as oxides, which are reduced to their metallic states during the reaction, thereby acting as catalysts[34]. Fe_2O_3 was not fully reduced during the reaction but was partially reduced to a suboxide (represented by $Fe_{0.94}O$)[45]. This structure was also detected in the pre-reduced catalysts. Combined with the H_2-TPR results shown in **Fig. 7(g)**, it is evident that 5Fe-0.8Ni/A-Al_2O_3 is more readily reduced. The reduction peaks for this catalyst appear in the low-temperature region with narrower peak widths compared to 5Fe-0.8Ni/Al_2O_3, due to the better dispersion of metal oxides on the support surface.[46] The presence of defective structures in non-integer-ratio oxides may also influence the volatile matter reaction, as these oxides tend to adsorb oxygenated substances at defect sites, thereby affecting coke deposit formation.[47] As demonstrated by the experimental results, this directs the adsorbed polymerized volatiles toward the formation of "soft" coke. In the case of pre-reduced catalysts, the volatiles reforming reaction disrupts the formed nickel-iron alloy, resulting in coke deposits that resemble those produced by 5Fe or 0.8Ni catalysts.

The fresh and used 5Fe-0.8Ni/Al_2O_3 and 5Fe-0.8Ni/A-Al_2O_3 catalysts were characterized by XPS, and the Fe fine spectra are shown in **Fig. 7(b-c)**. The two fresh catalysts exhibit similar Fe valence states and chemical environments,[48] with Fe^{2+} present in the Fe_3O_4 formed from Fe_2O_3 during the high-temperature calcination. The used 5Fe-0.8Ni/A-Al_2O_3 catalyst contains a higher proportion of metallic Fe, consistent

View Article Online
DOI: 10.1039/D5GC02932E

with the XRD and H_2-TPR characterization results. The Ni fine spectra are presented in **Fig. 7(e-f)**. While the two fresh catalysts display similar Ni valence states and chemical environments, the used 5Fe-0.8Ni/A-Al_2O_3 catalyst shows a significantly higher metallic nickel content compared to the used 5Fe-0.8Ni/Al_2O_3. This aligns with existing studies indicating that Ni is more prone to catalyzing coke deposits. Furthermore, this study highlights Ni's ability to promote the formation of "soft" coke with a low degree of unsaturation.

As shown in **Fig. 7(h-i)**, the acidic sites of fresh and used 5Fe-0.8Ni/Al_2O_3 and 5Fe-0.8Ni/A-Al_2O_3 were characterized by NH_3-TPD. For used catalysts, the pyrolysis of surface materials affects the TCD signal, resulting in peaks around 400 °C. 5Fe-0.8Ni/A-Al_2O_3 primarily contains weak acid sites, evidenced by desorption peaks below 200 °C, and medium-strong acid sites, with desorption peaks between 200 °C and 400 °C. In contrast, 5Fe-0.8Ni/Al_2O_3 exhibits only a few weak acid sites. After the reaction, 5Fe-0.8Ni/A-Al_2O_3 lost medium-strong acid sites and some weak acid sites, indicating that coke deposits formed predominantly on medium-strong acid sites. These medium-strong acid sites, characterized by higher polarity, preferentially adsorb large polar substances such as oxygenated compounds.[49] The polar environment inhibits chemical reactions that reduce polarity, thereby suppressing the formation of "hard" coke. For 5Fe-0.8Ni/Al_2O_3, there was no significant change in the acidic sites before and after the reaction. This suggests that coke deposits primarily form on less polar sites, facilitating the formation of "hard" coke. Notably, while 5Fe-0.8Ni/A-Al_2O_3 showed substantial acid site loss after single use, activity decline remained insignificant even

View Article Online
DOI: 10.1039/D5GC02932E

after three cycles. This demonstrates that "soft" coke formed on lost acid sites continues to preferentially adsorb tar, simultaneously reducing harmful byproducts while delaying active site poisoning and deactivation.

The XPS C 1s spectra of used 5Fe-0.8Ni/A-Al_2O_3 and used 5Fe-0.8Ni/ A-Al_2O_3 are shown in **Fig. 8(a)**. The C 1s spectra contain organic contaminant carbon species such as C-C, C-O, and C=O, making it difficult to extract specific sample information solely from a single carbon spectrum. Therefore, a comparative analysis of the XPS C 1s spectra between the two samples is necessary. Compared to the spent 5Fe-0.8Ni/A-Al2O3 catalyst, the C-C peak (284.8 eV) of the spent 5Fe-0.8Ni/Al_2O_3 exhibits poorer symmetry, indicating a higher content of sp^2-C on its surface. The peak observed at the higher binding energy region (290.9 eV) corresponds to a satellite peak arising from π-π* electronic excitations in graphitic carbon,[50] suggesting that the coke deposits on this catalyst are more graphitized and thus "harder" in nature. In contrast, the used 5Fe-0.8Ni/A-Al_2O_3 demonstrates a higher intensity of the C=O peak (288.8 eV), implying that its coke deposits are "softer".

View Article Online
DOI: 10.1039/D5GC02932E

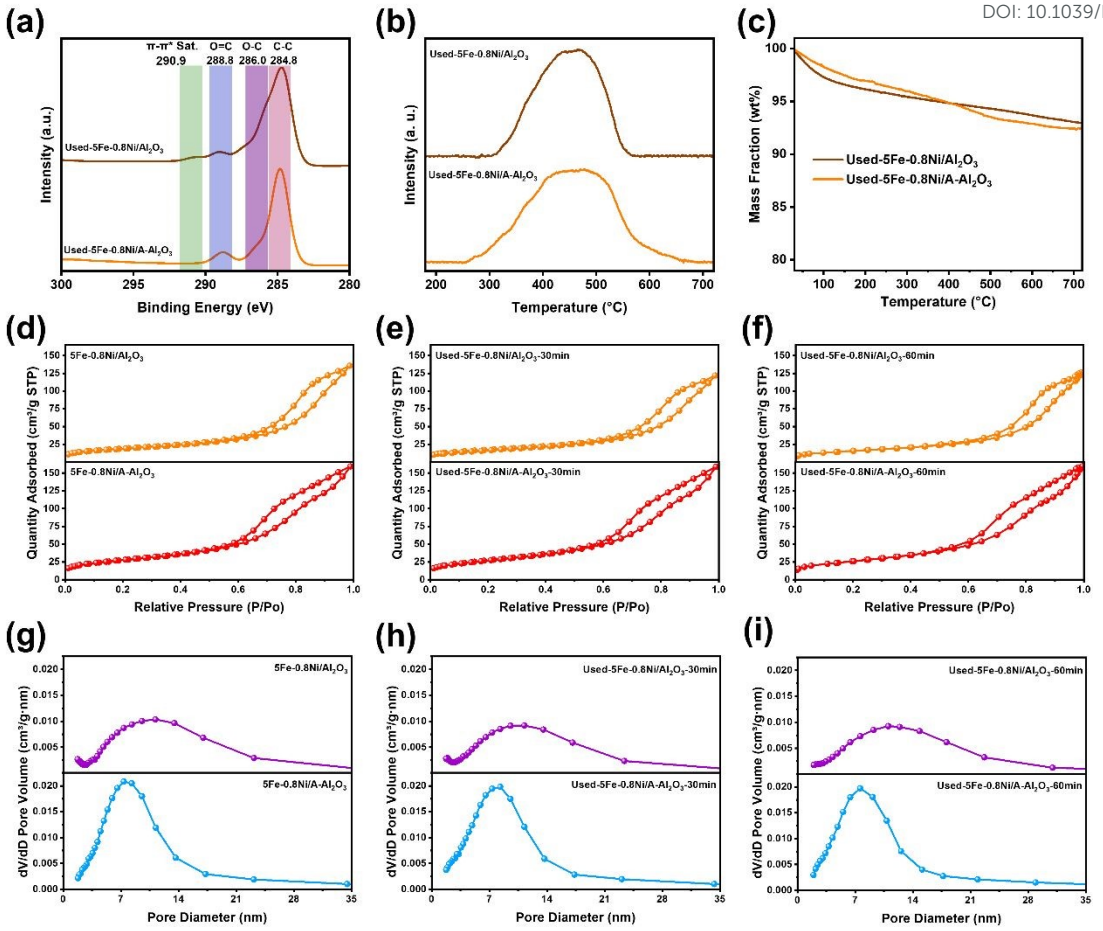

Fig. 8. C 1s XPS spectra of used catalysts (a). O_2-TPO curves of used 5Fe-0.8Ni/ Al_2O_3 and used 5Fe-0.8Ni/A-Al_2O_3 (b). TGA curves of used 5Fe-0.8Ni/ Al_2O_3 and used 5Fe-0.8Ni/A-Al_2O_3 in the air atmosphere (c). N_2 adsorption-desorption curves of fresh/used catalysts (d-f), pore size distribution curves of fresh/used catalysts (g-i).

As shown in **Fig. 8(b-c)**, O_2-TPO and air-TGA were conducted on the used 5Fe-0.8Ni/Al_2O_3 and used 5Fe-0.8Ni/A-Al_2O_3 catalysts. The O_2-TPO profiles revealed that the coke deposits on the used 5Fe-0.8Ni/A-Al_2O_3 exhibited a lower initial oxidation temperature and a broader oxidation peak, indicating a higher quantity of coke deposits with more diverse structural characteristics. The weight loss observed in the low-temperature region of TGA was attributed to moisture absorption by the samples, while the trend above 200 °C correlated well with the O_2-TPO results. The used 5Fe-0.8Ni/A-

View Article Online
DOI: 10.1039/D5GC02932E

Al_2O_3 demonstrated a greater weight loss rate, consistent with the research conclusion that the "softer" the coke deposits, the greater their mass.

The fresh, used-30min, and used-60min 5Fe-0.8Ni/Al_2O_3 and 5Fe-0.8Ni/A-Al_2O_3 were characterized by N_2 adsorption-desorption. The specific surface area, average pore diameter, and pore volume are summarized in **Table 3**. The adsorption-desorption curves are shown in **Fig. 8(d-f)**, and the pore size distributions are presented in **Fig. 8(g-i)**. The adsorption-desorption curves of both catalysts exhibit Type IV isotherms, and their mesoporous nature is confirmed by the pore size distribution. The H3-type hysteresis loop indicates that the pore structure of the catalysts is highly irregular, consisting of slit-like mesopores formed by the aggregation of layered structures.[51] As the reaction proceeds, the peak intensity of the pore size distribution decreases, and the average pore size slightly increases after prolonged reaction time, which is attributed to the partial blockage of catalyst pores by coke deposits formed during the reaction. However, the two catalysts exhibit different trends in specific surface area and pore volume changes: for 5Fe-0.8Ni/Al_2O_3, as the reaction time increased, the specific surface area decreased from 67.81 m^2/g to 62.58 m^2/g (30 min) and further to 57.72 m^2/g (60 min), while the pore volume decreased from 0.2096 cm^3/g to 0.1885 cm^3/g and further to 0.1855 cm^3/g. This was due to the catalyst being enveloped by coke deposits. In contrast, 5Fe-0.8Ni/A-Al_2O_3 showed no significant changes in specific surface area and pore volume; the 30-min-used catalyst (99.26 m^2/g) exhibits a slightly higher specific surface area than the fresh catalyst (98.89 m^2/g), suggesting that the coke deposits formed on this catalyst have a highly disordered structure. These results

View Article Online
DOI: 10.1039/D5GC02932E

indicate that the structural characteristics of "soft" coke deposits differ from those of "hard" coke deposits.

Table 3. Physical properties of different catalysts.

Catalyst	Surface Area (m^2/g)	Pore Volume (cm^3/g)	Average pore (nm)
5Fe-0.8Ni/Al_2O_3	67.81	0.2096	12.37
5Fe-0.8Ni/A-Al_2O_3	98.89	0.2463	9.96
Used-5Fe-0.8Ni/Al_2O_3-30min	62.58	0.1885	12.05
Used-5Fe-0.8Ni/A-Al_2O_3-30min	99.26	0.2454	9.89
Used-5Fe-0.8Ni/Al_2O_3-60min	57.72	0.1855	13.54
Used-5Fe-0.8Ni/A-Al_2O_3-60min	97.42	0.2448	10.26

The fresh and used 5Fe-0.8Ni/Al_2O_3 and 5Fe-0.8Ni/A-Al_2O_3 catalysts were characterized by TEM (are shown in **Fig. 9**). The fresh catalyst exhibited clear lattice fringes at higher magnification, whereas the used catalyst showed blurred features due to coverage by amorphous coke deposits,[52] which are macromolecular polymers rather than crystalline materials. For 5Fe-0.8Ni/Al_2O_3, the number of dark regions increased after use, with distinct contours of encapsulating coke deposits.[53] As the reaction proceeds, coke deposits may migrate into the pores, causing catalyst deactivation.[54] In contrast, 5Fe-0.8Ni/A-Al_2O_3 formed striped coke after the reaction, exhibiting much weaker encapsulation. This indicates that "hard" coke has a compact structure, whereas "soft" coke is more loosely structured. Based on the fixed-bed reactor scale-up experiments and N_2 adsorption-desorption of catalysts, it can be concluded that "hard"

View Article Online
DOI: 10.1039/D5GC02932E

coke deposits contribute significantly more to catalyst deactivation than "soft" coke deposits.

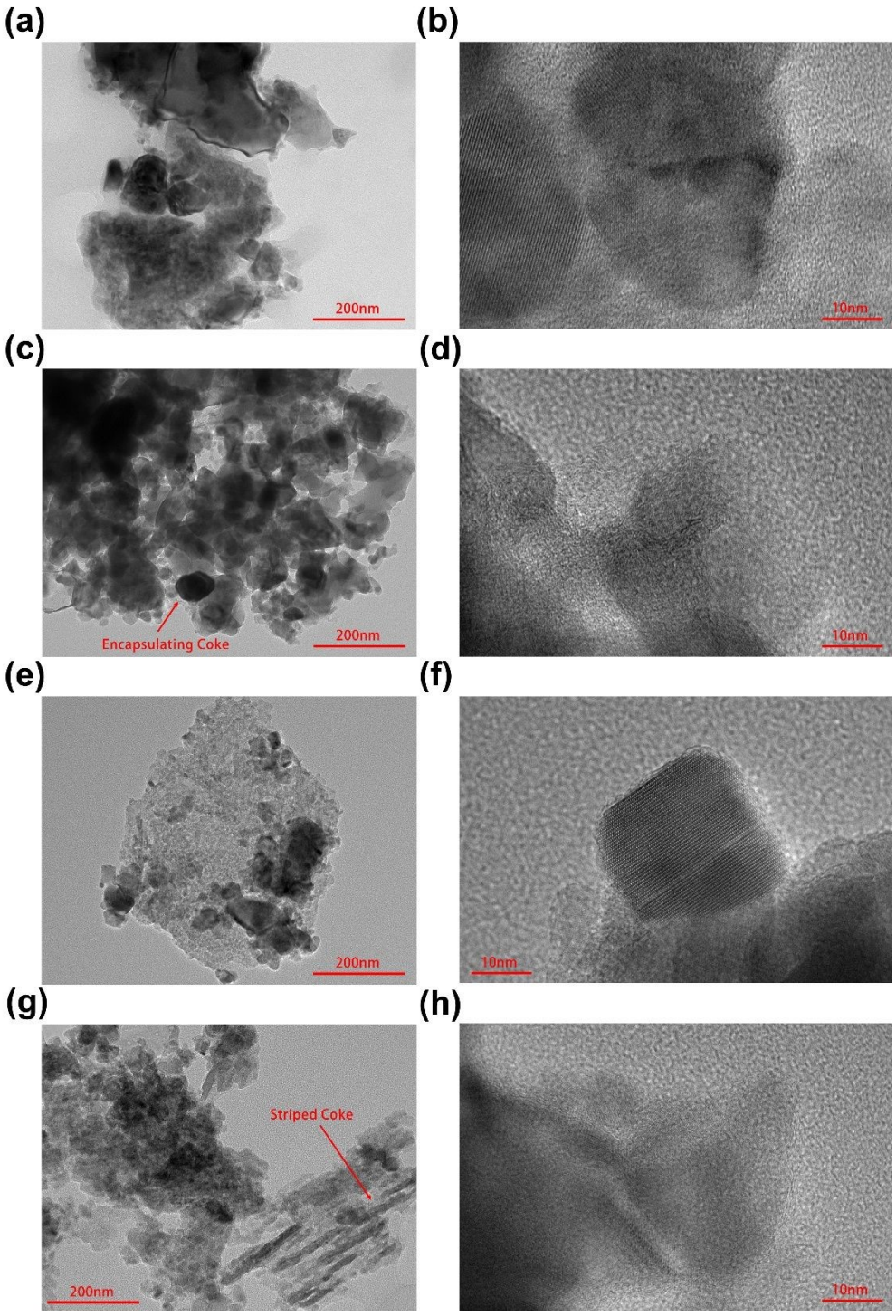

Fig. 9. TEM images of 5Fe-0.8Ni/Al_2O_3 (a-b), used-5Fe-0.8Ni/Al_2O_3 (c-d), 5Fe-0.8Ni/A-Al_2O_3 (e-f), and used-5Fe-0.8Ni/A-Al_2O_3 (g-h).

View Article Online
DOI: 10.1039/D5GC02932E

To further elucidate the relationship between the formation of "soft" coke with five-membered rings and catalyst properties, as shown in **Fig. 10(a-c)**, a weakly polar SiO_2-supported Fe-0.8Ni was tested in three consecutive cycles in a fixed-bed reactor. The coke content was quantified by TGA in the air atmosphere (**Table 1**). The used catalyst after the first cycle showed 2.98% weight loss in TGA, and Py-GC/MS analysis detected no five-membered ring structures in the coke deposits, indicating the formation of "hard" coke. Significant catalyst deactivation was observed with successive reaction cycles. For comparison, as shown in **Fig. 10(d-f)**, ZSM-5 with stronger surface polarity was evaluated under identical reaction conditions. Unlike Fe-0.8Ni/SiO_2, ZSM-5 exhibited much slower deactivation. The first-cycle used ZSM-5 catalyst showed 5.35% weight loss in TGA, and Py-GC/MS analysis revealed abundant branched aromatics and five-membered ring compounds. After three reaction cycles, oxidized compounds were detected in the coke deposits, indicating a decrease in their ability to convert oxidized compounds. Combined with fixed-bed reactor results from 5Fe-0.8Ni/Al_2O_3 and 5Fe-0.8Ni/A-Al_2O_3 systems, these findings demonstrate that the formation of "soft" coke with five-membered rings requires strongly polar supports to adsorb molecular precursors, followed by subsequent transformation at metal sites. Compared to "hard" coke, this "soft" coke has a higher molecular weight but causes less catalyst deactivation.

View Article Online
DOI: 10.1039/D5GC02932E

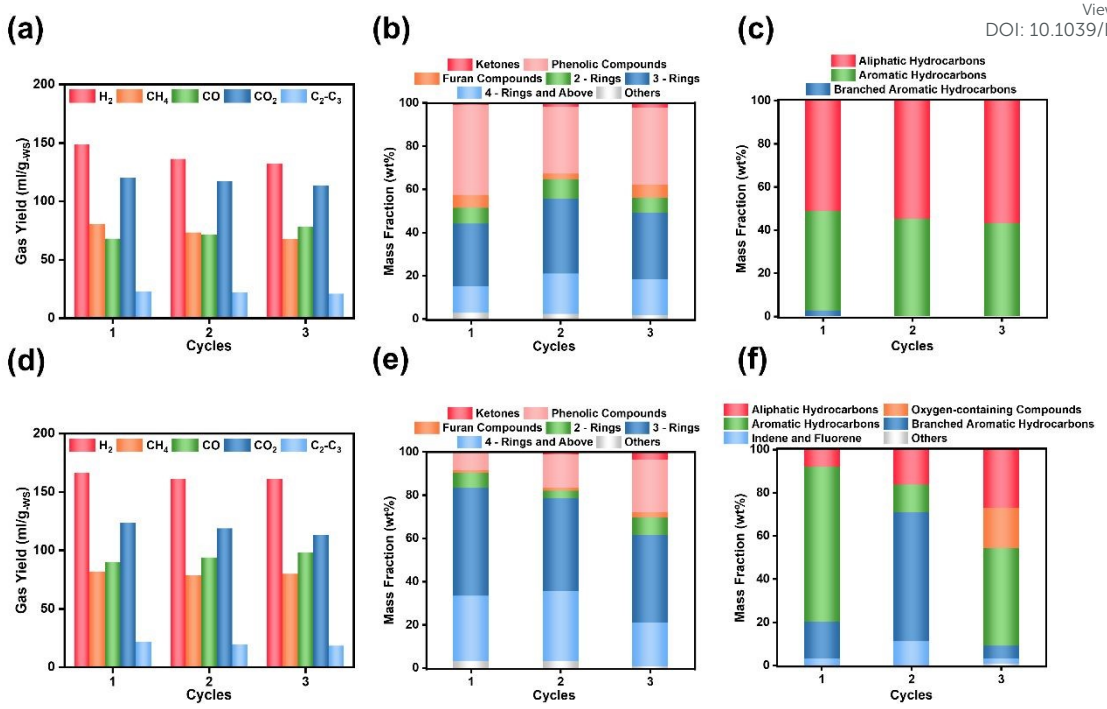

Fig. 10. Gas products (a and d). condensable fractions (b and e), and results of used-catalyst detection by Py-GC/MS for the catalyst after use (c and f), obtained by ex-situ catalytic pyrolysis of WS for volatiles reforming in the fixed-bed reactor.

3.3 Structural analysis and formation mechanism of coke deposits

Combining Py-GC/MS characterization of coke deposit structures with the various morphological characterizations of the catalysts, this work summarizes the reasonable structural fragments of the coke deposits and the evolution of the catalysts during the catalytic reaction. As illustrated in **Fig. 11(a)**, the molecular backward induction of fragments from coke deposits pyrolysis reveals that the structure of coke deposits includes not only graphite lamellae with six-membered rings but also irregular structures such as aliphatic groups, aromatic groups, and five-membered rings at the edges. These five-membered rings, embedded within the coke deposits, represent the

View Article Online
DOI: 10.1039/D5GC02932E

primary forms of low-unsaturated groups in "soft" coke deposits. **Fig. 11(b)** outlines the potential pathways for catalyst interaction with the pyrolytic volatiles of WS. The fresh catalyst model is represented by a spinel structure,[55] where O^{2-} forms the densest stacking, Fe^{3+} occupies the octahedral voids, and Ni^{2+} fills the tetrahedral voids of the oxygen lattice. Panel (I) depicts only the surface portion of this structure. During biomass pyrolysis, reducing molecules interact with the oxide fraction, producing reactive phases such as suboxides and metals, as shown in (II). Organic compounds in the pyrolyzed volatiles interact with these active phases, removing small molecules and generating highly unsaturated aromatic hydrocarbons adsorbed on the catalyst surface, as illustrated in (III). The volatiles continue to interact with the catalyst, and the adsorbed material provides a platform for polymer growth. This process involves the adsorption of various organics and the removal of small molecules, facilitating polymerization in the presence of the catalyst, as depicted in (IV) and (V). These panels illustrate the structure and formation of "soft" coke, which incorporates five-membered rings. Over time, as the reaction progresses, thermochemical reactions deoxygenate the oxygen-containing functional groups on the surface of "soft" coke. The aromatic and aliphatic groups then condense to form graphitic carbon layers, resulting in "hard" coke and ultimately leading to catalyst deactivation.

View Article Online
DOI: 10.1039/D5GC02932E

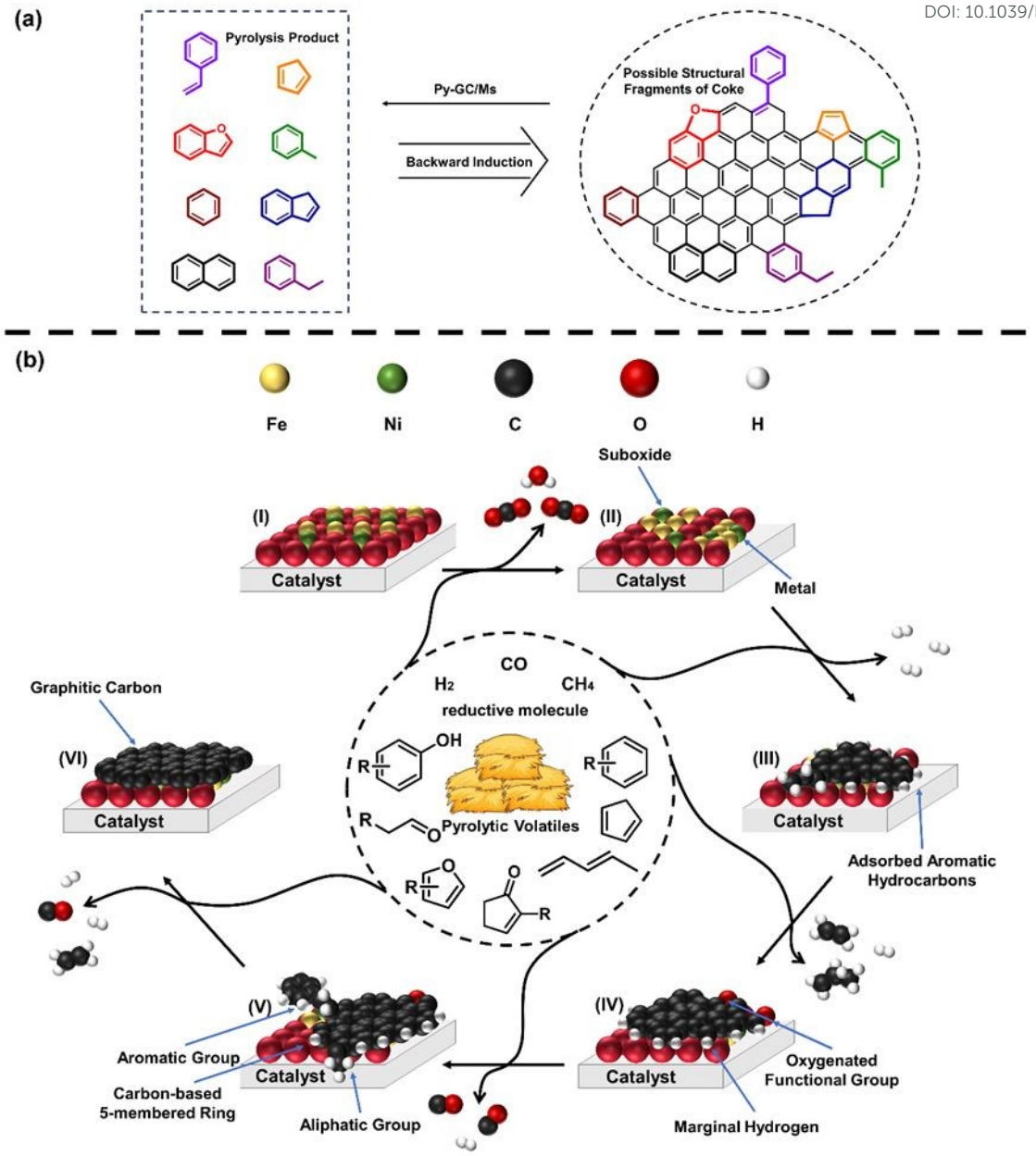

Fig. 11. Possible structure of the coke deposits on the catalysts inferred from the results of the Py-GC/MS analysis (a). Possible change paths of the coke and catalyst during operation (b).

The structure and formation mechanism of five-membered rings in "soft" coke deposits on catalysts have rarely been reported. To elucidate the formation mechanism of "soft" coke, particularly the key intermediates involved in five-membered ring

View Article Online
DOI: 10.1039/D5GC02932E

formation, model compounds were selected, and experiments were conducted to identify the initial origins of these intermediates compared to real biomass. Glucose, representative of sugar-based polymers such as cellulose and hemicellulose, and guaiacol, representative of phenol-based polymers such as lignin, were subjected to fast pyrolysis using Py-GC/MS to explore their primary volatiles. As shown in **Table 4**, the results were compared with those from WS. Furans were primarily produced from cellulosic compounds,[56] while lignin mainly generated phenols and highly unsaturated hydrocarbons.[57] The mass spectrum of the biomass pyrolysis product exhibits a base peak at m/z 83, as shown in **Fig. S10**. Comparison with the standard spectrum identified this substance as cyclopentenone, and its methyl-substituted derivative was also detected. These compounds were also observed during glucose pyrolysis and are presumed to originate from methylfuran and its derivatives, which are formed through the dehydration and decarbonylation of dehydration products of glucose. The fragmentation patterns of these compounds are similar, supporting this hypothesis. Guaiacol produced cyclopentadienone analogs, detected as dimers formed via the Diels-Alder reaction. These analogs likely arise from the cleavage of catechol, produced by guaiacol demethylation, followed by CO removal.[58] Pyrolysis of real biomass yielded five-membered ring structures such as indene, which are presumed to derive from the aforementioned five-membered ring compounds. Cyclopentenones may react and condense with hydrocarbon compounds to form indene.

Table 4. Volatile components produced by WS, glucose, and guaiacol in fast pyrolysis experiments were analyzed using Py-GC/MS.

Compounds	WS	Glucose	Guaiacol
	12.19%	38.07%	1.6%
Furan Compounds	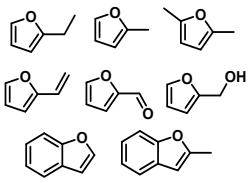	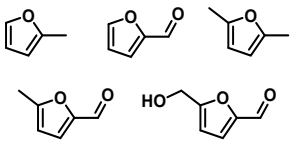	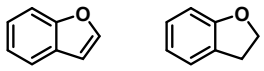
	14.24%	16.76%	15.23%
Carbonyl Compounds	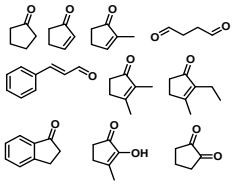	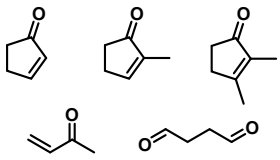	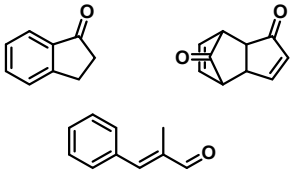
	33.9%	3.12%	70.28%
Phenolic Compounds	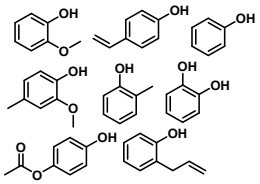	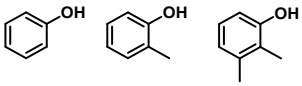	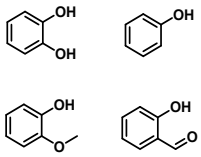
	14.97%	7.25%	11.45%
Aliphatic Hydrocarbons	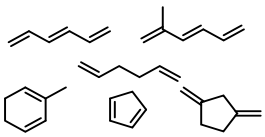	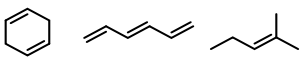	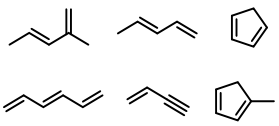
	17.04%	13.92%	1.6%
Aromatic Hydrocarbons	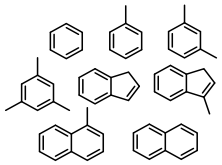	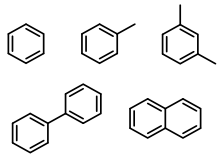	
	7.66%	20.88%	--
Others	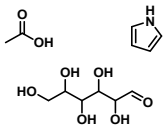	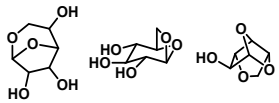	

Based on the experimental results (**Fig. 1** and **Fig. 2**) and the reasonable assumption that the five-membered ring structure in coke deposits originates from the adsorption of aromatic hydrocarbons with five-membered rings in the volatiles, fast

View Article Online
DOI: 10.1039/D5GC02932E

pyrolysis experiments of model compounds catalyzed by 5Fe-0.8Ni/A-Al_2O_3 were conducted using Py-GC/MS. The results are presented in **Table 5**, and the analysis of catalysts after reactions with real biomass and model compounds is detailed in **Table S9**. Glucose pyrolysis products, including condensed glucose, were completely converted in the presence of the catalyst, with a significant decrease in cyclopentenone content. This indicates that the reaction rate of furan compound conversion to cyclopentenones is slower than the polymerization and conversion of cyclopentenones into final products. The catalyst facilitates the subsequent conversion of cyclopentenones, and indene compounds, not previously detected in direct pyrolysis experiments, were identified. The content of aliphatic hydrocarbons decreased significantly, and no chain aliphatic hydrocarbons were detected, confirming that the conversion of cyclopentenones to aromatic hydrocarbons such as indene requires reactions with aliphatic hydrocarbons and catalytic cyclization and dehydrogenation. Phenols produced by guaiacol cleavage were fully converted in the presence of the catalyst. The primary products included dibenzofurans, formed by the reaction of phenols with aliphatic hydrocarbons, and a small amount of cyclopentadienone dimer. The cyclopentadienone dimer can undergo decarbonylation in the presence of the catalyst, either cracking to produce aliphatic hydrocarbons or further dehydrogenating and cyclizing to form aromatic hydrocarbons. Additionally, the catalyst catalyzes methyl migration on the methoxy group of guaiacol, producing various methyl-substituted aromatic hydrocarbons. The benzyl radical, stabilized by conjugation with the benzene ring, is more reactive than a conventional methyl group and may serve as

View Article Online
DOI: 10.1039/D5GC02932E

a site for further polymerization. WS comprises approximately 40-50% cellulose, 20-25% hemicellulose, and 15-20% lignin.[59] Cyclic ketones detected in real biomass pyrolysis experiments were predominantly cyclopentenones. Based on these findings, cyclopentenones derived from cellulose/hemicellulose pyrolysis are considered key intermediates for forming five-membered ring structures in coke deposits, and these model compound experiments can be extrapolated to most cellulose/hemicellulose-rich biomass materials. Biomass with high cellulose/hemicellulose content tends to form "soft" coke deposits during catalytic reforming, while lignin-rich biomass preferentially generates "hard" coke that accelerates catalyst deactivation. Compounds such as indene and fluorene, containing five-membered rings, likely form through reactions involving cyclopentenones. For PAHs with more than two rings, their aromaticity is weaker than that of benzene, making them prone to undergo cyclization reactions at the edges to form five-membered rings.[60] In contrast, benzene, with its stronger aromaticity, is less likely to participate in such reactions. Therefore, it is proposed that indene is generated from compounds that already possess a five-membered ring. Catalytic fast pyrolysis experiments with cyclopentenone and hexadiene as model compounds confirmed that cyclopentenone can react with unsaturated hydrocarbons to produce aromatic hydrocarbons with five-membered rings, which may serve as precursors for coke deposits.

Table 5. Products of catalytic fast pyrolysis experiments of glucose, guaiacol, and the mixture of cyclopentenone and hexadiene using 5Fe-0.8Ni/A-Al_2O_3 in Py-GC/MS.

Compounds	Glucose	Guaiacol	Cyclopentenone Hexadiene
Furan Compounds	50.05% 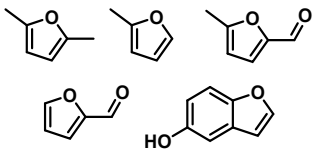	8.91% 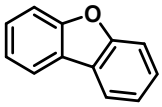	--
Carbonyl Compounds	5.42% 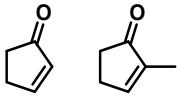	2.02% 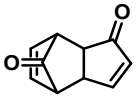	30.1% 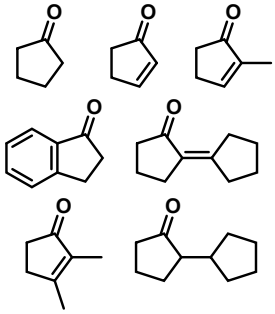
Phenolic Compounds	10.91% 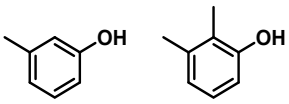	--	--
Aliphatic Hydrocarbons	4.35% 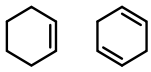	24.22% 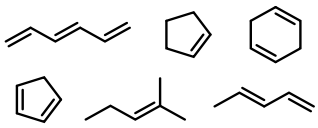	40.18% 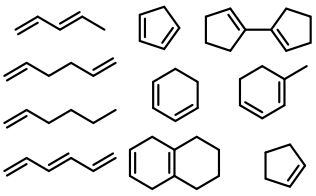
Aromatic Hydrocarbons	29.27% 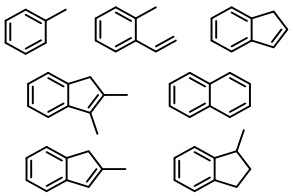	64.88% 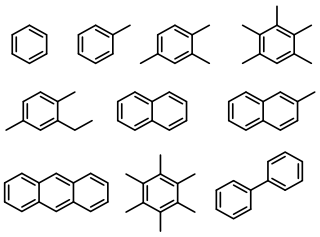	29.73% 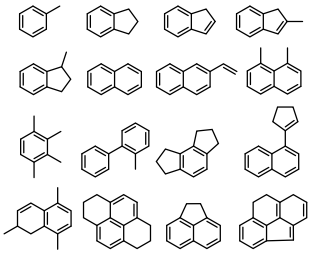

View Article Online
DOI: 10.1039/D5GC02932E

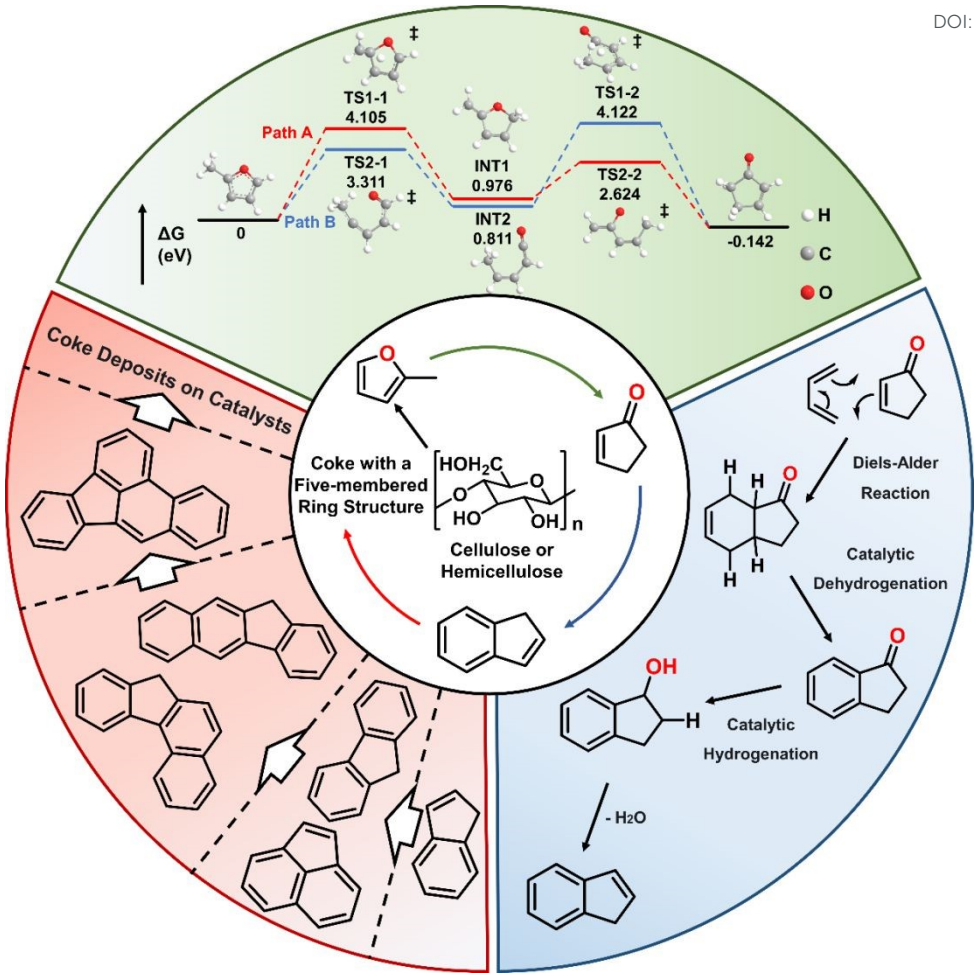

Fig. 12. Possible mechanism analysis of the formation of the five-membered ring structure in coke deposits.

Based on the experimental results (**Fig. 1-6, Table 3-5**), the mechanism for the formation of coke deposits with five-membered ring structures on the catalyst was deduced, as illustrated in **Fig. 12**. This mechanism comprises three main steps: (1) the isomerization of methyl furan to the five-membered ring intermediate cyclopentenone, (2) the conversion of cyclopentenone to aromatic hydrocarbons such as indenes, and (3) the polymerization of aromatic hydrocarbons with five-membered ring structures to form coke deposits containing five-membered rings. While the generation of furans from cellulose and hemicellulose in biomass has been extensively studied and will not

View Article Online
DOI: 10.1039/D5GC02932E

be elaborated here,[56] the conversion of methyl furan to cyclopentenone, though noted in many studies, lacks a clear reaction mechanism. Therefore, this work proposes two possible pathways: (1) **Path A**: Methyl furan undergoes a σ-migration reaction to form intermediate INT1, followed by 1,2-bond cleavage to produce a free radical. This radical undergoes internal flipping and cyclization to form cyclopentenone. (2) **Path B**: Methyl furan undergoes 1,5-bond cleavage and hydrogen migration to form intermediate INT2, followed by hydrogen migration and cyclization to yield cyclopentenone.

To determine the more plausible mechanism, density functional theory (DFT) calculations were performed to optimize the transition states (TS1-1, TS1-2, TS2-1, TS2-2) and calculate the reaction energy barriers. Kinetic model analysis (as shown in the **SI**) revealed that the apparent activation energy of **Path A** is lower than that of **Path B**. Additionally, **Path B** involves excessive spatial distortion, making **Path A** the more favorable mechanism. The calculated dipole moments were 0.9113 Debye for methylfuran and 3.9191 Debye for cyclopentenone, respectively, indicating that the reaction is more likely to occur in more polar media and that cyclopentenone is more readily adsorbed on strongly polar supports. Cyclopentenone, derived from methyl furan, reacts with conjugated dienes produced during biomass pyrolysis in a Diels-Alder reaction catalyzed by the catalyst, forming hexahydroindenone. Subsequent catalytic dehydrogenation produces dihydroindenone, which undergoes catalytic hydrogenation to yield dihydroindenol. Finally, thermal dehydration generates indenes. All intermediates in this reaction sequence could be detected by Py-GC/MS. Indene

View Article Online
DOI: 10.1039/D5GC02932E

compounds adsorb onto the catalyst and undergo ring expansion reactions with low-carbon hydrocarbons in the biomass pyrolysis volatiles, accompanied by the removal of H_2, leading to the formation of PAHs featuring five-membered ring structures (**Fig. 12** illustrates the structures detected via Py-GC/MS). This ring expansion reaction may occur on either the benzene ring or the five-membered ring.[40, 61] As the molecular weight increases, these compounds gradually become more difficult to desorb, progressively clogging the catalyst's pores and covering active sites, ultimately resulting in the formation of coke deposits on the catalysts.

A comparison of this work with the existing literature is presented in **Table S10**. Traditional coke deposit research focuses on physical morphology and site blockage.[17, 31] In recent years, research on the structure and mechanism of coke deposits has gradually shifted toward the molecular level. Consistent with many other studies, this work considers coke deposits to be not merely graphite carbon layers, but rather a type of macromolecular compound with functional groups at the edges. However, existing research on 'soft' coke deposits often focuses on the fatty and oxygen-containing functional groups at the edges of the six-membered ring[14, 15] and does not pay attention to the structure of the carbon layer itself. Existing work has observed five-membered ring compounds in volatile matter,[62] but the conclusion is that this type of compound will be converted into a six-membered ring graphite carbon layer, without proposing that the structure and reaction mechanism of the five-membered ring remain on the coke deposits. Studies using model compounds have shown that the source of aromatic carbon is not solely lignin, which has phenolic structures as its structural units; furan

View Article Online
DOI: 10.1039/D5GC02932E

compounds can also serve as sources.[15] This work combines real biomass with model compounds to propose, for the first time, a carbon layer structure containing five-membered rings, and investigates its formation mechanism and its effect on catalyst deactivation.

4. Conclusions

The formation of coke deposits is a major cause of catalyst deactivation in biomass pyrolysis volatiles reforming processes. Understanding the structural characteristics and formation mechanisms of coke deposits, as well as their impact on reforming reactions, is crucial for developing coke-resistant catalysts to address catalyst deactivation issues. In this work, we employed Py-GC/MS to analyze small molecules derived from pyrolyzed coke deposits, and through reverse deduction, we proposed for the first time that "soft" coke contains not only edge aliphatic and aromatic groups but also five-membered rings with saturated carbon atoms. Through a series of systematic experiments, we investigated the role of the catalyst in transforming coke deposits and the influence of different coke structures on catalytic performance. Supports with higher polarity guided the formation of "soft" coke deposits, while bimetallic catalysts, compared to monometallic catalysts, formed new active phases and suppressed the formation of graphitic carbon layers. Significantly, "soft" coke containing five-membered rings has a negligible impact on catalyst deactivation; instead, its formation facilitates the conversion and reduction of harmful tar byproducts. However, prolonged reaction leads to catalytic promotion of dehydrogenation and deoxygenation processes

View Article Online
DOI: 10.1039/D5GC02932E

that convert "soft" coke into "hard" coke, ultimately resulting in catalyst deactivation. In addition, catalysts on other supports and non-metallic catalysts were employed to validate the above conclusions. Real biomass and model compound pyrolysis experiments identified cyclopentenones, produced from cellulose and hemicellulose pyrolysis, as key intermediates for the formation of five-membered ring structures in "soft" coke. Combining experimental results with theoretical calculations, a chemical reaction mechanism for the formation of "soft" coke was proposed. This mechanism starts from methylfuran, progresses through cyclopentenone and indene, and ultimately forms "soft" coke with five-membered ring structures. This work provides a detailed reference for studying coke deposits in practical biomass reactions. Building upon these research findings, our team's future research focus will be on the development of coke-resistant catalysts capable of directing the structural formation of coke deposits.

Author contributions

Wenkai Lang: data curation and Writing - original draft. Jin Deng: formal analysis and Writing - original draft. Xin Liu and Zaiyu Yang: Software and Visualization. Ruxia Zhang and Honghong Liu: Supervision. Keyuan Sun and Shenfu Yuan: Writing - review editing.

Conflicts of interest

The authors declare no conflict of interest.

View Article Online
DOI: 10.1039/D5GC02932E

Acknowledgements

We greatly acknowledge the Reserve Program for Young and Middle-aged Academic and Technical Leaders in Yunnan Province (Grant NO. 202205AC160031), the Yunnan Fundamental Research Project (Grant NO. 202501AS070077, 202301BF070001-010), the Scientific Research Fund Project of Yunnan Education Department (2025Y0014), and the Scientific Research and Innovation Project of Postgraduate Students in the Academic Degree of Yunnan University (KC-24248746).

References

1. D. Shindell and C. J. Smith, *Nature*, 2019, **573**, 408-411.
2. Y. Queneau and B. Han, *Innovation*, 2022, **3**, 100184.
3. H. D. Setiabudi, M. A. A. Aziz, S. Abdullah, L. P. Teh and R. Jusoh, *International Journal of Hydrogen Energy*, 2020, **45**, 18376-18397.
4. Y. Xie, Y. Su, P. Wang, S. Zhang and Y. Xiong, *Fuel Processing Technology*, 2018, **182**, 77-87.
5. F. Lin, M. Xu, K. K. Ramasamy, Z. Li, J. L. Klinger, J. A. Schaidle and H. Wang, *Acs Catalysis*, 2022, **12**, 13555-13599.
6. Y. Zhao, S. Yuan, Y. Zhou, X. Xie and J. Deng, *Journal of Analytical and Applied Pyrolysis*, 2023, **173**, 106041.
7. S. A. Theofanidis, V. V. Galvita, H. Poelman, R. Batchu, L. C. Buelens, C. Detavernier and G. B. Marin, *Applied Catalysis B-Environmental*, 2018, **239**,

View Article Online
DOI: 10.1039/D5GC02932E

502-512.

8. H. Sun, D. Feng, S. Sun, Q. Wei, Y. Zhao, Y. Zhang, M. Xie and Y. Qin, *Fuel Processing Technology*, 2021, **224**, 107007.

9. E. Heracleous, E. Pachatouridou, A. M. Hernandez-Gimenez, H. Hernando, T. Fakin, A. L. Paioni, M. Baldus, D. P. Serrano, P. C. A. Bruijnincx, B. M. Weckhuysen and A. A. Lappas, *Journal of Catalysis*, 2019, **380**, 108-122.

10. X. Yang, S. Wang, K. Zhang and Y. He, *Fuel*, 2021, **287**, 119547.

11. A. Ochoa, B. Aramburu, B. Valle, D. E. Resasco, J. Bilbao, A. G. Gayubo and P. Castano, *Green Chemistry*, 2017, **19**, 4315-4333.

12. Q. Zhang, Z. Jiang, Y. Zhang, X. Xu, Y. Yang, Y. Qin, L. Song, Y. Mei and Y. Zu, *Applied Catalysis B-Environment and Energy*, 2025, **362**, 124722.

13. C. Liu, X. Chen, X. Liu, C. Cui, Z. Zhou, L. Jia and F. Qi, *Angewandte Chemie-International Edition*, 2021, **60**, 2643-2647.

14. B. Wang, J. Hu, W. Chen, C. Chang, S. Pang and P. Li, *Fuel*, 2024, **357**, 129859.

15. P. Liu, W. Shao, Z. Yang, J. Yang, L. Jia, Y. Pan, Z. Zhou, Y. Chen and F. Qi, *Acs Catalysis*, 2023, **13**, 12227-12237.

16. K. Wang, K. H. Kim and R. C. Brown, *Green Chemistry*, 2014, **16**, 727-735.

17. Y. Zhao, S. Yuan, J. Deng, C. Li, Y. Feng, X. Xie and N. Li, *Journal of Analytical and Applied Pyrolysis*, 2022, **168**, 105778.

18. S. Azeem, M. Safdar, R. Aslam, B. Wang, I. Ziani, S. Ansar and F. Sher, *Process Safety and Environmental Protection*, 2024, **187**, 962-973.

View Article Online
DOI: 10.1039/D5GC02932E

19. S. Zhang, W. Chen, L. Yang, T. Xie, W. Li, D. Yu and Y. Fang, *Journal of Solid State Chemistry*, 2021, **303**, 122503.

20. M. Guisnet and P. Magnoux, *Applied Catalysis a-General*, 2001, **212**, 83-96.

21. S. Du, J. A. Valla and G. M. Bollas, *Green Chemistry*, 2013, **15**, 3214-3229.

22. F. Lou, J. Wang, J. Sima, J. Lei and Q. Huang, *Journal of Hazardous Materials*, 2023, **459**, 132098.

23. W.-H. Chen, C.-W. Wang, G. Kumar, P. Rousset and T.-H. Hsieh, *Bioresource Technology*, 2018, **259**, 469-473.

24. P. Zhou, S. Xiong, Y. Zhang, H. Jiang, Y. Chi and L. Li, *International Journal of Hydrogen Energy*, 2017, **42**, 18181-18188.

25. L. He, Q. Yao, R. Cao, L. Wang, W. Wang, D. Ma, M. Sun and X. Ma, *Chemical Engineering Journal*, 2024, **492**, 152410.

26. G. San Miguel, J. Aguado, D. P. Serrano and J. M. Escola, *Applied Catalysis B-Environmental*, 2006, **64**, 209-219.

27. Y. He, Y. Zhao, M. Chai, Z. Zhou, M. Sarker, C. Li, R. Liu, J. Cai and X. Liu, *Renewable & Sustainable Energy Reviews*, 2020, **119**, 109604.

28. D. Prat, A. Wells, J. Hayler, H. Sneddon, C. R. McElroy, S. Abou-Shehada and P. J. Dunn, *Green Chemistry*, 2016, **18**, 288-296.

29. G. Elordi, M. Olazar, G. Lopez, P. Castano and J. Bilbao, *Applied Catalysis B-Environmental*, 2011, **102**, 224-231.

30. S. Zhang, J. Wang, L. Ye, S. Li, Y. Su and H. Zhang, *Chemical Engineering Journal*, 2023, **454**, 140072.

View Article Online
DOI: 10.1039/D5GC02932E

31. J. Wang, S. Zhang, L. Ye, Y. Xiong and H. Zhang, *Fuel Processing Technology*, 2023, **250**, 107897.

32. N. Amarnath, S. Shukla and B. Lochab, *Acs Sustainable Chemistry & Engineering*, 2018, **6**, 15151-15161.

33. J. Liu, H.-d. Sun, S.-H. Hu, B. Hu, Z.-m. Fang, J.-h. Li, Z.-x. Zhang and Q. Lu, *Energy*, 2024, **311**, 133480.

34. J. Deng, Y. Zhou, Y. Zhao, L. Meng, T. Qin, X. Chen, K. Li and S. Yuan, *Energy*, 2022, **244**, 122602.

35. S. Yang, Z. Huang, P. Wu, Y. Li, X. Dong, C. Li, N. Zhu, X. Duan and D. D. Dionysiou, *Applied Catalysis B-Environmental*, 2020, **260**, 118129.

36. J. Ren, J.-P. Cao, F.-L. Yang, Y.-L. Liu, W. Tang and X.-Y. Zhao, *Acs Sustainable Chemistry & Engineering*, 2021, **9**, 17186-17206.

37. R. Padhye, A. J. A. Aquino, D. Tunega and M. L. Pantoya, *Acs Applied Materials & Interfaces*, 2016, **8**, 13926-13933.

38. D. M. Santosa, C. Zhu, F. Agblevor, B. Maddi, B. Q. Roberts, I. V. Kutnyakov, S.-J. Lee and H. Wang, *Acs Sustainable Chemistry & Engineering*, 2020, **8**, 5156-5164.

39. G. Li, Z. Wang, L. Zuo, T. Zhang, W. Xiao, T. Yang, O. Tursunov, N. Zhao and Y. Zhou, *Bioresource Technology*, 2024, **409**, 131259.

40. X. Shi, Q. Wang and A. Violi, *Fuel*, 2021, **283**, 119023.

41. Y. Liu, L. Liu and L. Hong, *Catalysis Today*, 2017, **281**, 352-359.

42. J. Liu, Y. Ma, D. Zhu, T. Xia, Y. Qi, Y. Yao, X. Guo, R. Ji and W. Chen,

View Article Online
DOI: 10.1039/D5GC02932E

Environmental Science & Technology, 2018, **52**, 2677-2685.

43. A. R. Stanton, K. Iisa, C. Mukarakate and M. R. Nimlos, *Acs Sustainable Chemistry & Engineering*, 2018, **6**, 10030-10038.

44. K. Zheng, H. Han, S. Hu, Q. Ren, S. Su, Y. Wang, L. Jiang, J. Xu, H. Li, Y. Tong and J. Xiang, *Energy*, 2023, **267**, 126536.

45. T. Yamashita, T. Nakada and K. Nagata, *Metallurgical and Materials Transactions B-Process Metallurgy and Materials Processing Science*, 2007, **38**, 185-191.

46. D. Nielsen, Q. Gao, T. V. W. Janssens, P. N. R. Vennestrom and S. Mossin, *Journal of Physical Chemistry C*, 2023, **127**, 12995-13004.

47. X. Qi, T. Lin, Y. An, X. Wang, D. Lv, Z. Tang and L. Zhong, *Acs Catalysis*, 2023, **13**, 11566-11579.

48. M. C. Biesinger, B. P. Payne, A. P. Grosvenor, L. W. M. Lau, A. R. Gerson and R. S. C. Smart, *Applied Surface Science*, 2011, **257**, 2717-2730.

49. D.-H. Liu, H.-L. He, J.-J. Wang, S.-Y. Zhou, T. Zeng, X.-Y. Gao, Y. Xiao, X. Yi, A. Zheng, Y.-B. Zhang and Z. Li, *Green Chemistry*, 2021, **23**, 9974-9981.

50. A. V. Shchukarev and D. V. Korolkov, *Central European Journal of Chemistry*, 2004, **2**, 347-362.

51. L. Jin, H. Li, Y. Zhang, D. Peng, Z. Sun and A. Zhang, *Particle & Particle Systems Characterization*, 2023, **40**, 2200199.

52. N. Luo, H. Cai, X. Li, M. Guo, C. Wang, X. Wang, P. Hu, Z. Cheng and J. Xu, *Journal of Materials Chemistry A*, 2022, **10**, 15136-15145.

View Article Online
DOI: 10.1039/D5GC02932E

53. D. Xu, Y. Xiong, J. Ye, Y. Su, Q. Dong and S. Zhang, *Chemical Engineering Journal*, 2020, **392**, 123728.

54. J. Wu, M. Dai, B. Yang, P. Li, C. Wang, G. Wu, X. Jiang, S. Yu, W. Li, X. Li, T. Zhao, D. Yang, R. Chu and X. Meng, *Chemical Engineering Journal*, 2024, **482**, 148974.

55. A. Srifa, R. Kaewmeesri, C. Fang, V. Itthibenchapong and K. Faungnawakij, *Chemical Engineering Journal*, 2018, **345**, 107-113.

56. L. Chen, Y. Liao, Z. Guo, Y. Cao and X. Ma, *Journal of Cleaner Production*, 2019, **232**, 1309-1320.

57. S. Ghysels, L. E. Arteaga-Perez, A. E. Leon, T. Menares, S. Backx, S. Mangelinckx and F. Ronsse, *Acs Sustainable Chemistry & Engineering*, 2023, **11**, 13765-13777.

58. P. Hemberger, V. B. F. Custodis, A. Bodi, T. Gerber and J. A. van Bokhoven, *Nature Communications*, 2017, **8**, 15946.

59. B. Liu, L. Liu, B. Deng, C. Huang, J. Zhu, L. Liang, X. He, Y. Wei, C. Qin, C. Liang, S. Liu and S. Yao, *International Journal of Biological Macromolecules*, 2022, **222**, 1400-1413.

60. L. Zhao, M. Prendergast, R. I. Kaiser, B. Xu, U. Ablikim, W. Lu, M. Ahmed, A. D. Oleinikov, V. N. Azyazov, A. H. Howlader, S. F. Wnuk and A. M. Mebel, *Physical Chemistry Chemical Physics*, 2019, **21**, 16737-16750.

61. Z.-H. Ma, S. Li, X.-Q. Dong, M. Li, G.-H. Liu, Z.-Q. Liu, F.-J. Liu, Z.-M. Zong, X.-S. Cong and X.-Y. Wei, *Fuel*, 2023, **334**, 126637.

View Article Online
DOI: 10.1039/D5GC02932E

62. J. Du, T. Shen, J. Hu, F. Zhang, S. Yang, H. Liu and H. Wang, *Energy*, 2023, **277**, 127733.

View Article Online
DOI: 10.1039/D5GC02932E

Data availability statement

All relevant data are within the manuscript and its Additional files.